Chemical Geology 365 (2014) 54–68

Contents lists available at ScienceDirect

Chemical Geology

journal homepage: www.elsevier.com/locate/chemgeo

Trace element budgets and (re-)distribution during subduction-zone ultrahigh pressure metamorphism: Evidence from Western Tianshan, China

Yuanyuan Xiao [a,b,*], Yaoling Niu [a,c,**], Huaikun Li [d], Huichu Wang [d], Xiaoming Liu [e], Jon Davidson [a]

[a] Department of Earth Sciences, Durham University, Durham DH1 3LE, UK
[b] Institute of Earth Sciences, Academia Sinica, 128 Academia Road, Section 2, Nangang, Taipei 11529, Taiwan
[c] Institute of Oceanology, Chinese Academy of Sciences, Qingdao 266071, China
[d] Tianjin Institute of Geology and Mineral Resources, Tianjin 300170, China
[e] State Key Laboratory of Continental Dynamics, Department of Geology, Northwest University, Xi'an 710069, China

ARTICLE INFO

Article history:
Received 2 April 2012
Received in revised form 11 December 2013
Accepted 12 December 2013
Available online 21 December 2013

Editor: L. Reisberg

Keywords:
Subduction-zone metamorphism
Element (re-)distributions
Arc magmatism
Mantle compositional heterogeneity

ABSTRACT

We have conducted an LA-ICP-MS *in situ* trace element study of garnet, epidote group minerals, phengitic muscovite and paragonite in rocks of basaltic and sedimentary protolith from an ultrahigh pressure metamorphic belt along Western Tianshan, China. The data are used to evaluate the capacity of these minerals for hosting incompatible elements in response to subduction-zone metamorphism (SZM). The results confirm existing studies in that the presence and stability of these minerals largely control the geochemical behaviors of elements during SZM.

We found that redistribution of rare earth elements (REEs), Th and U into newly-formed minerals during progressive SZM precludes the release of these elements from the down-going ocean crust, which contradicts the common perception in models of slab-dehydration and flux-melting. This suggests that additional processes, such as the involvement of supercritical fluids or hydrous melts formed at depth are required to supply these elements to the mantle wedge for arc magmatism. In addition, the ready release of large ion lithophile elements (LILEs) by different minerals, and the high immobility of REEs in rocks of basaltic protolith indicate that the contribution of altered ocean crust after SZM may not be responsible for the correlated Sr–Nd (Hf) isotope systematics observed in oceanic basalts. That is, subducted ocean crust that has gone through SZM cannot be the major source material for ocean island basalts.

1. Introduction

Subduction zones are the most important tectonic environment on Earth in terms of the extent, magnitude, and diversity of mass exchange between the Earth's exterior and the deep mantle. Subduction zones provide a highly selective physical and chemical filter, conceptualized as the "subduction factory" (*e.g.*, Tatsumi and Kogiso, 2003). The main process in the subduction factory is metamorphism. In fact, it is the subduction-zone metamorphism (SZM) that is considered to trigger subduction-zone magmatism (*e.g.*, Tatsumi, 1986; Peacock, 1990; McCulloch and Gamble, 1991), while residual material passing through the SZM contributes to mantle chemical and isotopic heterogeneities (*e.g.*, Hofmann and White, 1982; Zindler and Hart, 1986; Niu and O'Hara, 2003). Therefore, it is crucial to understand the genuine behaviors of chemical elements in response to the SZM in order to obtain an improved understanding of subduction-zone magmatism and chemical geodynamics.

Seafloor materials which have experienced hydrothermal alteration and weathering become highly altered (termed "altered oceanic crust" or AOC; Staudigel et al., 1995; Kelley et al., 2003). The AOC undergoes dehydration in subduction zones, releasing fluids which selectively carry fluid-soluble or mobile elements (*e.g.*, large ion lithophile elements, LILEs) into the overlying mantle wedge, while leaving the fluid-insoluble or immobile elements (*e.g.*, high field strength elements, HFSEs) in the "residual" slab. Melting of the so preferentially enriched mantle wedge is then expected to produce basaltic rocks with the characteristic arc signatures (McCulloch and Gamble, 1991). The residual slab retaining the immobile elements is thus transported into the deep mantle. Because of the often different behaviors of radioactive parent and radiogenic daughter elements, the residual slab with altered parent/daughter (P/D) ratios during the SZM will determine the nature and extent of mantle isotopic variability as reflected in oceanic basalts (*e.g.*, enriched mantle I [EMI], enriched mantle II [EMII], and high "μ"

* Correspondence to: Y. Xiao, Institute of Earth Sciences, Academia Sinica, 128 Academia Road, Section 2, Nangang, Taipei 11529, Taiwan. Tel.: +886 2 2783 9910x618.
** Correspondence to: Y. Niu, Department of Earth Sciences, Durham University, Durham DH1 3LE, UK. Tel.: +44 19 1334 2311.
E-mail addresses: xiaoyy@earth.sinica.edu.tw, xiaoy806@gmail.com (Y. Xiao), yaoling.niu@durham.ac.uk (Y. Niu).

0009-2541/$ – see front matter © 2013 Elsevier B.V. All rights reserved.
http://dx.doi.org/10.1016/j.chemgeo.2013.12.005

[HIMU; $\mu = {}^{238}U/{}^{204}Pb$]; Zindler and Hart, 1986; Weaver, 1991; Hofmann, 1997). While the above analysis is reasonable, Niu and O'Hara (2003) argued that the Sr–Nd–Hf isotopic systematics of global ocean island basalts (OIB) recorded no prior subduction-zone histories of OIB sources.

The recent recognition of ultrahigh pressure (UHP) hydrous minerals exceeding the amphibole stability field (*e.g.*, lawsonite, phengite; Poli and Schmidt, 1995; Schmidt and Poli, 1998) indicates a geochemically more complex SZM process than previously thought, involving not only discontinuous dehydration but also continuous reactions (Poli and Schmidt, 1995). Furthermore, recent experimental studies and studies on natural rocks have revealed the strong capacity of these UHP minerals for hosting petrologically important trace elements (*e.g.*, Hermann, 2002; Feineman et al., 2007; El Korh et al., 2009). Hence, the retention of these elements may result in a complex element transfer process during the SZM.

With varied geothermal conditions in different subduction zones, the stability of minerals, fluid compositions (aqueous fluids, hydrous melts or supercritical fluids; Kessel et al., 2005; Hermann et al., 2006; Mibe et al., 2011) and reaction kinetics (Becker et al., 2000; Carlson, 2002; John et al., 2004; Beinlich et al., 2010) may all affect elemental behaviors during the SZM (*e.g.*, Spandler et al., 2003). In addition, the quantity of fluids and the nature of fluid flow (*e.g.*, channels/veins, high permeable mélange zones; Zack and John, 2007; John et al., 2008) may also exert important controls on the interactions between fluids and metamorphic rocks during the SZM. The higher the fluid/wall rock ratio is, the more likely the elements can migrate (Bebout, 2007) and the mobile elements could be homogenized. Therefore, studies of geochemical behaviors of specific elements in response to the SZM and their controls are essential, especially for natural rocks that have experienced the SZM in an open system. Microanalysis techniques (*e.g.*, Laser Ablation-Inductively Coupled Plasma Mass Spectrometry, LA-ICP-MS) allow *in situ* trace element analysis of minerals with high precision and accuracy, which should improve our understanding of elemental behaviors and the mineralogical controls during the SZM (*e.g.*, El Korh et al., 2009; Schmidt et al., 2009).

In this study, we focus on the distributions of LILEs and rare earth elements (REEs) in different mineral assemblages of blueschist- to eclogite-facies metamorphic rocks of basaltic and sedimentary protoliths from the UHP metamorphic belt of Western Tianshan, China, in order to understand trace element behaviors in response to the mineral stability at different metamorphic stages along a specific *P–T* path. Evidenced by the occurrence of coesite, this metamorphic belt of Western Tianshan in recent studies is considered to have experienced >2.5 GPa subduction-zone metamorphism (Lü et al., 2008, 2009; Lü and Zhang, 2012). Considering that our eclogitic samples are from this UHP metamorphic belt, they can be used to evaluate the geochemical consequences of SZM at depths greater than 75 km, even though coesite has not been found in the samples we studied (Xiao et al., 2012).

2. Field geology, petrography and bulk-rock geochemical studies: a review

The Western Tianshan Metamorphic Belt (WTMB) in northwest China has experienced Carboniferous UHP metamorphism (Lü et al., 2008, 2009; Lü and Zhang, 2012). This belt is located along the South Central Tianshan Suture, which defines the south boundary of the Yili-Central Tianshan Plate (Fig. 1; *e.g.*, Zhang et al., 2001; Gao and Klemd, 2003), and is thought to continue westwards into Kazakhstan (Volkova and Budanov, 1999). The WTMB marks the convergent margin associated with successive northward subduction of the South Tianshan Silurian-Devonian-seafloor and the Tarim Plate (*e.g.*, Gao et al., 1999; Gao and Klemd, 2003).

We have studied rock samples of both basaltic and sedimentary protoliths metamorphosed to blueschist and eclogite facies, in which retrograde alteration is common to varying extents (sample locations are given in Fig. 1b and Table DR1). Metamorphic rocks of sedimentary protoliths contain higher modal abundances of quartz and white micas (including phengitic muscovite and paragonite) and display stronger foliations. The eclogite *sensu stricto* (where garnet + omphacite > 70 vol.% of the bulk rock; *e.g.*, TS02-3B, TS02-15A, TS02-17b and TS02-32A) is mainly composed of garnet and omphacite, with varying amounts of glaucophane, white micas, epidote group minerals, quartz, carbonate and rutile. The blueschist contains more glaucophane, while epidote amphibolite contains more retrograde amphibole with (sodic–)calcic component and epidote group minerals. No obvious HP-UHP dehydration/transport veins have been found in these studied rocks. Only some small veins cutting through all the early-formed metamorphic minerals, likely produced after the SZM, are observed on a thin section scale.

On the basis of detailed petrography, especially of the mineral assemblage (Table DR1) and the textural relationships (*e.g.*, Fig. 2), together with the estimated metamorphic *P–T* path for coesite-bearing eclogite from WTMB by Lü et al. (2009), a schematic *P–T* path for rocks of basaltic protolith from WTMB is given in Fig. 3. We divided four stages with different representative mineral assemblages, including prograde blueschist facies, UHP eclogite facies, retrograde eclogite facies and epidote amphibolite facies. The box-shaped lawsonite pseudomorphs (replaced by paragonite and clinozoisite, sometimes with albite; Fig. 2a) are common in garnet porphyroblasts, especially in their core–mantle portions. The replacement of dissolved (clino)zoisite by newly-crystallized omphacite and garnet (*e.g.*, Fig. 2b) corresponds to the reaction of 13 Gln + 6 Czs = 9 Prp + 26 Jd + 12 Di + 19 Coe/Qz + 16 H_2O (see the caption to Fig. 2 for mineral abbreviations), forming amoeboid crystal boundaries (John et al., 2008) and a 'sponge' texture. These textural relationships, together with the occurrence of glaucophane, clinozoisite and omphacite inclusions in garnet, point to the prograde blueschist facies, stage 1 in Fig. 3. The characteristic mineral assemblage at this stage is mainly composed of Lws + Czs + Gln + Omp + Grt + Ph + Pg + Rt. Although no coesite has been found in our samples, considering the occurrence of coesite and the absence of diamond in eclogites from Western Tianshan in others' studies (Lü et al., 2008, 2009), the peak metamorphic condition estimated by Lü et al. (2009; 2.4–2.7 GPa and 470–510 °C) is adapted here as stage 2 (Fig. 3), with the model peak mineral assemblage of Grt + Omp + Lws + Ph + Coe + Rt. The presence of large chloritoid poikiloblasts in sample TS02-01, which points to a pressure of ~2.2–2.4 GPa (Pawley and Holloway, 1993; Lü et al., 2009), is also consistent with the UHP at the peak metamorphic condition. On the other hand, the replacement of lawsonite inclusions by paragonite and clinozoisite in garnet indicates the breakdown of lawsonite, which may happen during retrograde eclogite facies (from stage 2 to stage 3 in Fig. 3), although the timing of this reaction remains debatable. For example, Gao et al. (1999), Gao and Klemd (2003) and Spandler et al. (2003) assumed that it happened during prograde metamorphism from lawsonite blueschist facies to eclogite facies. White micas, especially paragonite, may also be re-produced at this stage, and may replace the rim of garnet (Fig. 2a,f), or include the prior garnet (Fig. 2d), epidote and phengitic muscovite (Fig. 2e). The model mineral assemblage at stage 3 is Grt + Omp + Gln + Czs + Ph + Pg. From stage 3 (retrograde eclogite facies) to stage 4 (epidote amphibolite facies, Fig. 3), earlier glaucophane, omphacite, rutile and garnet were replaced by barroisite (Fig. 2g), retrograde epidote group minerals (Fig. 2c), titanite and chlorite (Fig. 2h). Therefore, the characteristic mineral assemblage becomes Czs + Ttn + Brs/Act + Ph + Chl + Ab.

We have previously used the Nb/Y *vs.* Zr/Ti diagram (Fig. DR1), an immobile trace-element equivalent of the TAS (total alkali *vs.* silica) diagram, to divide meta-basaltic rocks into three groups in terms of their large range of Nb/Y ratio within a small range of Zr/Ti (also see Table DR1 for grouping; Xiao et al., 2012). These three groups geochemically resemble OIB (Group 1), MORB contaminated by and/or mixing with continental or arc crust materials (Group 2), and depleted MORB

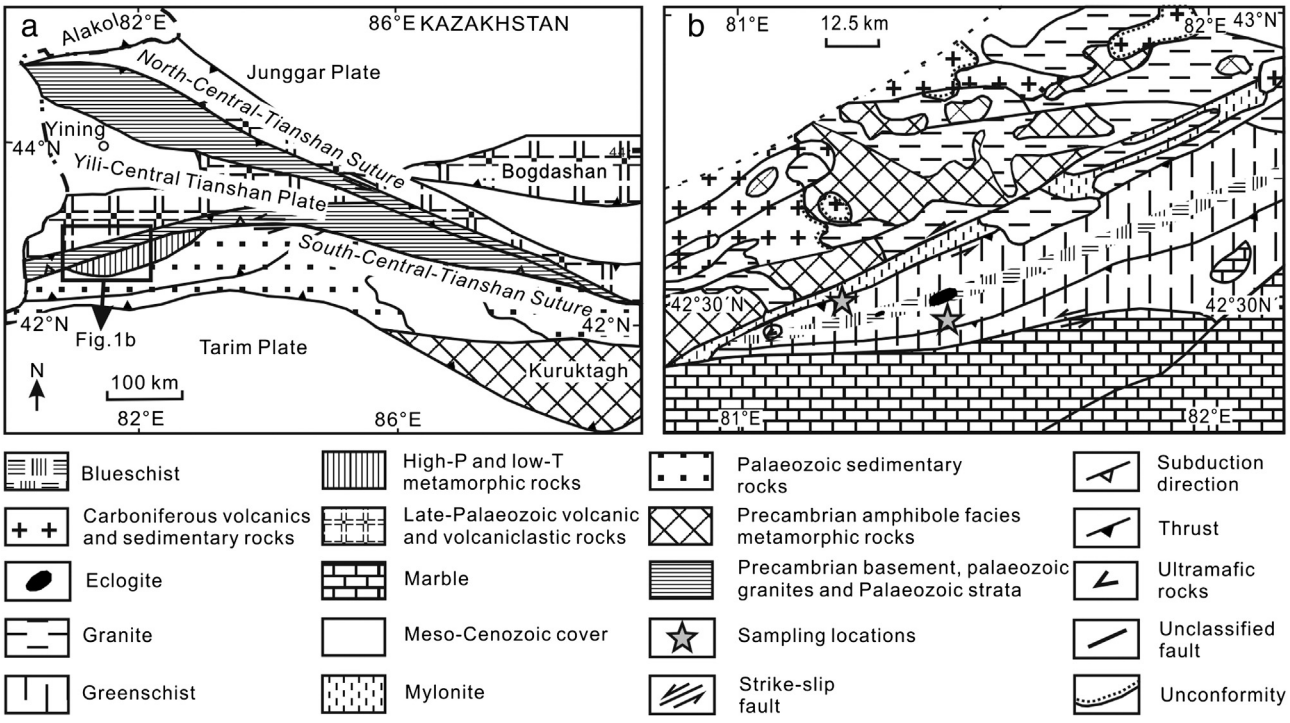

Fig. 1. (a) Geological map of Western Tianshan, China; (b) location of our samplings. After Gao and Klemd (2003) and Zhang et al. (2003).

(Group 3) (see Table DR2 and Fig. 4h for reference; similar geochemical variations of protolith rocks from Western Tianshan has also been reported by Ai et al., 2006). These rocks formed a tectonic mélange, the subduction of which resulted in the formation of the UHP metamorphic rocks from Western Tianshan. Through detailed studies on elemental correlations with assumed immobile elements (HFSEs) in bulk-rock compositions, we found that the behavior of Ba–Rb–Cs during the SZM is dependent on the lithologies; they are immobile in meta-sedimentary rocks but mobile in meta-basaltic rocks. REEs, HFSEs, Th and U are immobile while Pb and Sr are mobile in rock samples of both protoliths. Therefore, it was suggested that transport by hydrous fluids might be responsible for the enrichment of the mobile elements in arc lavas, but the immobile elements (*e.g.*, Th, U) may require different transport mechanisms such as the involvement of supercritical fluids or hydrous melts. The immobility of U in our studies (likely as U^{+4} *vs.* U^{+6}; Xiao et al., 2012) may indicate reduced conditions in subduction zones. Additionally, because of the poor correlations between P/D ratios in Sr–Nd (or Hf) isotope systems (*i.e.*, Rb/Sr *vs.* Sm/Nd or Lu/Hf) for representative eclogitic samples without or with minimum retrogressive overprints, it was proposed that the subducted ocean crust could not be the major source material for OIB (Xiao et al., 2012). However, the trace element distributions in minerals of the studied rocks and the controls on elemental behaviors remained unclear. Thus, in this paper, we analyzed the constituent mineral phases of these studied rocks using LA-ICP-MS, which allowed us to discuss elemental responses to mineral stability at each metamorphic stage along the *P–T* path (Fig. 3).

3. Analytical methods

Mineral compositions (both major and trace elements measured simultaneously) were analyzed using *in situ* LA-ICP-MS on polished thick (100 μm) "thin" sections using an Agilent 7500a equipped with GeoLas 2005 193 Eximer Laser sampler and a Varian 820-MS equipped with the same laser sampler. The repetition rate of laser ablation is 5–8 Hz, and the pit size ranges from 32 to 44 μm. During each analysis, the acquisition times for the background (gas blank) and the sample ablation were 20–30 s and 40–50 s respectively. United States Geological Survey (USGS) glasses BCR-2G, BIR-1G, BHVO-2G and one synthetic glass, GSE-1G, were all used as reference materials.

For mineral *in situ* trace element analysis, people traditionally choose to normalize to an element of known concentration in the sample, called "internal standard" (*e.g.*, prior analyzed using electron probe micro-analyzer, EPMA). In this study, for anhydrous minerals (*i.e.*, garnet, omphacite, rutile, titanite, feldspar), the concentrations of all elements of interest (both major and trace elements) were analyzed simultaneously through an internal standard-independent calibration method using an *ablation yield correction factor* (AYCF), together with multiple reference materials for external calibration (see Liu et al., 2008). The comparison with analytical data using scanning electron microscope–energy dispersive spectroscopy (SEM–EDS, see published data in Xiao et al., 2012) for major element contents of garnet and omphacite (Fig. DR2) shows that major element contents of anhydrous minerals analyzed using the AYCF LA-ICPMS method developed by Liu et al. (2008) are of high quality with $<\pm 10\%$ deviation (except for those elements with very low contents, *e.g.*, Na_2O, K_2O in garnet, FeO in omphacite). The apparent scatter for MgO and MnO in garnet (Fig. DR2a) reflects the compositional zoning. For hydrous minerals (amphiboles, epidote group minerals, phengitic muscovite, paragonite and chlorite), we used the traditional method, for which we chose ^{29}Si (analytical data of SEM–EDS, see Tables DR5–6, 9 and Xiao et al., 2012) as the internal standard. Off-line data reduction was performed using *ICPMSDataCal* (Liu et al., 2008). All other analytical details including instrument conditions are given in Liu et al. (2008). The analytical uncertainty and the precision are generally better than 5% and 10% respectively for data analyzed using both methods in terms of repeated analysis of GSE-1G (which contains high trace element concentrations ranging from several ppm to commonly 100s ppm; Guillong et al., 2005; Jochum et al., 2005) (Table DR3). During analysis we purposely avoided inclusions. To reconstruct the trace element budgets, we carefully determined mineral modal abundances using a James Swift automatic point counter (see details in Xiao et al., 2012).

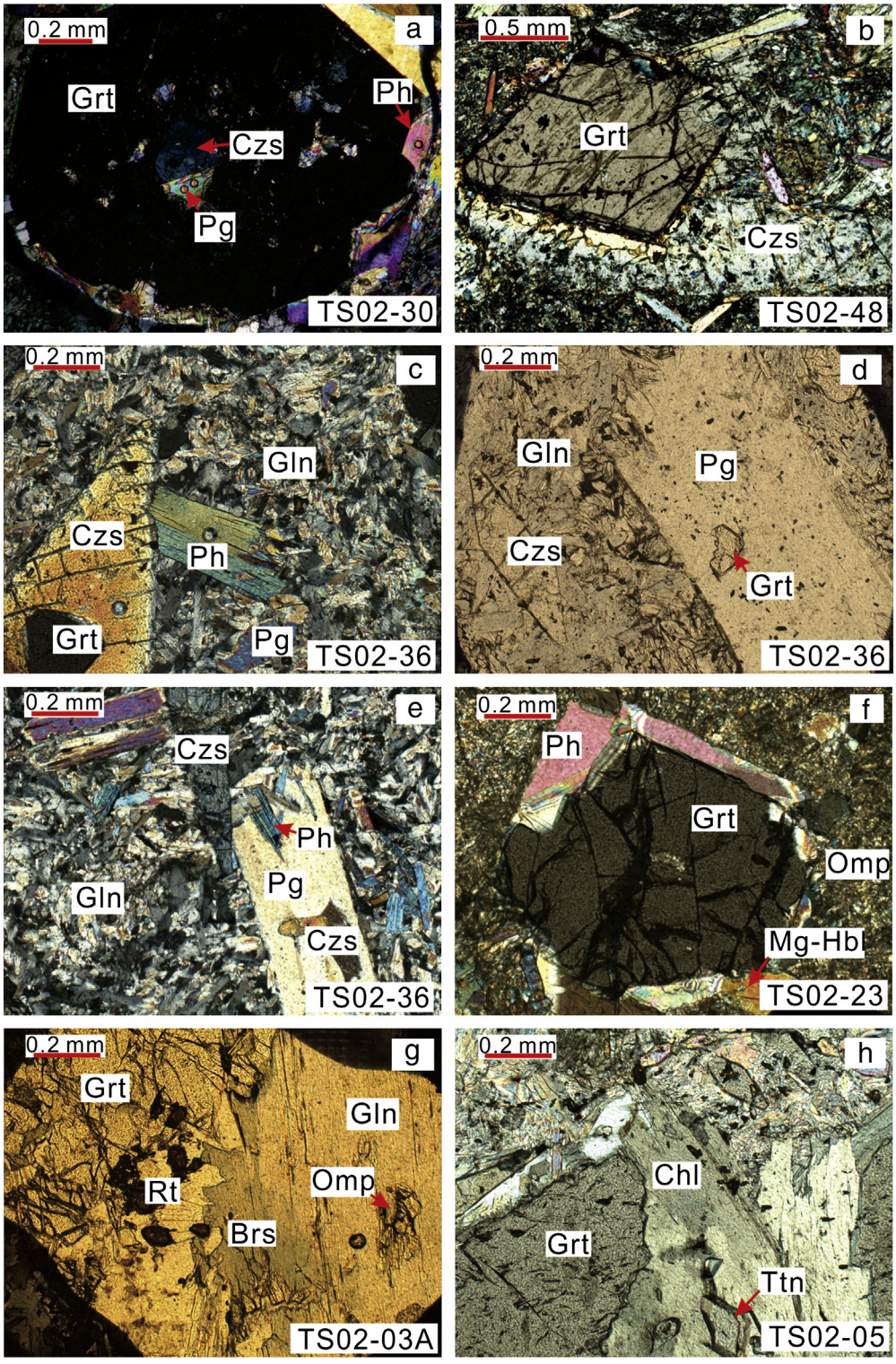

Fig. 2. Photomicrographs of representative rock samples from Western Tianshan, China. Except for (d) and (g) which were taken under plane polarized light, all the other photos are taken under cross polarized light. Mineral abbreviations used in this paper are referred to Whitney and Evans (2010), except: Ca—carbonate; Czs—(clino)zoisite. (a) Epidote-bearing eclogitic blueschist. Lawsonite pseudomorph preserved as box-shaped inclusions, consists of coexisting paragonite and clinozoisite in garnet. One mica grain has replaced the rim of garnet, probably reflecting the rehydrating process during retrograde metamorphism. (b) Omphacitite. One idioblastic garnet grain has grown at the expense of prograde clinozoisite nearby, resulting in a resorption grain boundary at the rim of the latter. (c) Epidote blueschist. One garnet is preserved as an inclusion in well-crystallized rhombic epidote. (d) One paragonite porphyroblast with a relic garnet inclusion probably reflects the rehydration during retrograde metamorphism. (e) Epidote and phengitic muscovite inclusions preserved in a paragonite porphyroblast indicate that the paragonite is most likely produced through the retrograde rehydration process while epidote and phengitic muscovite inclusions are formed at earlier metamorphic stages. (f) Epidote blueschist. The rim of garnet has been replaced by phengitic muscovite and Mg-hornblende. (g) Eclogitic blueschist. Glaucophane has been overprinted by a barroisite overgrowth rim. An omphacite relict is also included. (h) Retrograde blueschist. Together with chlorite, a titanite grain with a good prismatic crystal shape has largely replaced garnet.

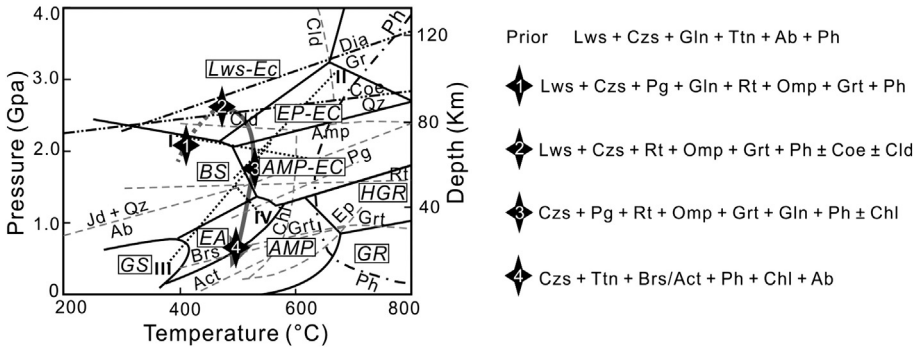

Fig. 3. Schematic phase diagram and mineral assemblages at each metamorphic stage for rocks of basaltic protoliths from UHP metamorphic belt of Western Tianshan, China. Metamorphic facies boundaries are referred to Liou et al. (2004). The dark gray curve with four diamonds is a schematic *P–T* path for our rocks of basaltic protoliths based on the detailed petrography (*e.g.*, Fig. 2). Each diamond represents a metamorphic stage, including prograde blueschist facies (stage 1), UHP eclogite facies (stage 2), retrograde eclogite facies (stage 3) and epidote amphibolite facies (stage 3). The related typical mineral assemblages for each stage are given on the right. Abbreviations: GS—greenschist facies; BS—blueschist facies; EA—epidote amphibolite facies; AMP—amphibolite facies; EC—eclogite; GR—granulite facies; HGR—high pressure granulite facies. Mineral abbreviations are as used in Fig. 2. Dotted lines labeled as I–IV represent four metamorphic reactions: reaction I—Pg = Ky + Jd_{50} + H_2O; II—Lws + Grt 1 = Czs + Di + Grt 2 + H_2O (Poli and Schmidt, 1997); III—Lws + Jd = 2 Czs + Pg + Qz + 6 H_2O or 4 Lws + Ab = 2 Czs + Pg + 2 Qz + 6 H_2O (Gao et al., 1999); IV—26 Jd + 12 Di + 9 Prp + 19 Qz + 15 H_2O = 13 Gln + 6 Czs (Zhang et al., 2002). The estimated peak metamorphic condition defined by Lü et al. (2009) is used in this study as stage 2. As evidenced by the occurrence of the box-shaped lawsonite pseudomorph (*e.g.*, Fig. 2a) and glaucophane and omphacite inclusions in garnet, it indicates the prograde blueschist facies metamorphism, stage 1. With the increase of temperature but the decrease of pressure, lawsonite may have been replaced by clinozoisite and paragonite (*e.g.*, Fig. 2a) through reaction II or reaction III, which we define as stage 3. The replacement of omphacite relicts by glaucophane (*e.g.*, Fig. 2g) and garnet relicts by epidote group minerals (*e.g.*, Fig. 2c) may indicate reaction IV. Together with the replacement of glaucophane by barroisite (*e.g.*, Fig. 2g) and garnet by chlorite and titanite (Fig. 2h) (probably through reaction 25 Gln + 6 Czs + 7 Qz + 14 H_2O = 50 Ab + 6 Tr + 9 Chl, Maruyama et al., 1986), it may suggest stage 4. The replacement of rutile by titanite also happened at this stage and may indicate reactions of Rt + Qz + Ca = Ttn + CO_2 (Niu and Lesher, 1991) and 3 Di + 2 Jd + H_2O + Qz + 3 Rt = 3 Ttn + Gln (Hernandez, 2001; van der Straaten et al., 2008).
Schematic phase diagram after Schmidt and Poli (1998), Poli and Schmidt (2002), Zhang et al. (2002, 2003), Xiao et al. (2012).

4. Mineral geochemistry

We analyzed garnet (Table DR4), epidote group minerals (Table DR5), white micas (both phengitic muscovite and paragonite; Table DR6), Ti-rich minerals (rutile and titanite; Table DR7), clinopyroxene (Table DR8), amphiboles (Table DR9), feldspar (Table DR8) and chlorite (Table DR9).

4.1. Major element composition

Garnet is almandine rich and shows pyrope component increase towards rims (*e.g.*, TS02-03A in Table DR4) in response to the prograde growth. Clinopyroxene is omphacitic (Table DR8). The composition of amphibole is variable, from calcic, sodic–calcic to sodic amphibole (amphibole classification follows Leake et al., 1997), and (sodic–)calcic amphibole is often present as a retrograde product. Some amphibole crystals show zoning, as evidenced by those with glaucophane cores overprinted by a rim of (sodic–)calcic amphibole. The composition of epidote group minerals is also variable. Allanite is present as the core of some clinozoisite crystals (Lavis, 2005). FeOt and Al_2O_3 are negatively correlated (not shown) due to the complementary Fe^{3+} Al substitution. Parts of epidote grains display zoning with Al_2O_3 increase (FeOt decrease) towards the rim, probably indicating increasing temperature (Deer et al., 1992).

4.2. Mineral trace element systematics

Experimental studies (*e.g.*, Feineman et al., 2007) and studies of natural rocks (*e.g.*, Spandler et al., 2003) have been used to determine preferential partitioning of chemical elements among coexisting minerals as a function of protolith composition and physical conditions. For example, phengitic muscovite has been found to be the major host of K, Ba, Rb and Cs (Sorensen et al., 1997; Becker et al., 2000; Melzer and Wunder, 2000; Zack et al., 2001); garnet is commonly enriched in HREEs (El Korh et al., 2009); epidote group minerals (*i.e.*, epidote, (clino)zoisite, allanite) and lawsonite are important hosts of REEs, Th, U, Pb and Sr (Nagasaki and Enami, 1998; Becker et al., 2000; Hermann, 2002; Spandler et al., 2003; Feineman et al., 2007); Sr could also reside in carbonate (van der Straaten et al., 2008; Beinlich et al., 2010); rutile and titanite host essentially all the Ti, Nb and Ta in the bulk rock (Stalder et al., 1998); zircon is responsible for hosting almost all the Zr and Hf in the rock (*e.g.*, Rubatto and Hermann, 2003). In the following, we discuss our mineral trace element data.

4.2.1. Garnet

Garnet is rich in middle (M-) to heavy (H-)REEs, up to ~10^3 times the chondrite values, but low in light (L-)REEs (Fig. 4a). The content of HREEs is variable even within one garnet crystal, commonly showing a general depletion of HREEs from core to rim (*e.g.*, one garnet inclusion in clinozoisite porphyroblast from TS02-53 in Fig. 4a, one garnet porphyroblast from TS02-03A in Table DR4). In the chondrite-normalized trace element diagram (Fig. 4a), some garnet grains show MREEs > HREEs. Considering the higher contents of MREEs relative to HREEs in some titanite crystals (*e.g.*, the one from TS02-43 in Fig. 4g), the scenarios of MREEs > HREEs in garnet may be resulted from redistribution of MREEs with the transition from titanite with high MREEs to rutile during the prograde metamorphism (also see Spandler et al., 2003; Konrad-Schmolke et al., 2008; Xiao et al., 2013). No compositional anomalies seem to be caused by distinctive textures (*e.g.*, inclusions preserved in clinozoisite in Fig. 2c or paragonite in Fig. 2d, relicts replaced by chlorite in Fig. 2h). This may suggest the strongest capability of garnet for hosting M-HREEs relative to other minerals (*e.g.*, King et al., 2004). The contents of Nb, Ta and Hf are low; mostly below the detection limit or only a few ppb (Zr can be up to several ppm).

4.2.2. White micas

Both phengitic muscovite and paragonite are rich in Li (generally 10s ppm) and Be (several ppm) (Table DR6). They also display high Ba–Rb–Cs (Fig. 5) and, to varying extent, Pb and Sr (Fig. 6a). Most phengitic muscovite and paragonite crystals have very low concentrations of Nb and Ta, but Nb can be up to a few ppm in several phengitic muscovite crystals.

4.2.2.1. Phengitic muscovite. Among the analyzed minerals, phengitic muscovite has the highest abundances of Ba, Rb, Cs and K, about 2–3 orders of magnitude higher than chondrite values (Fig. 4c). The highly variable LILEs with relatively constant K (not shown) suggest that K is

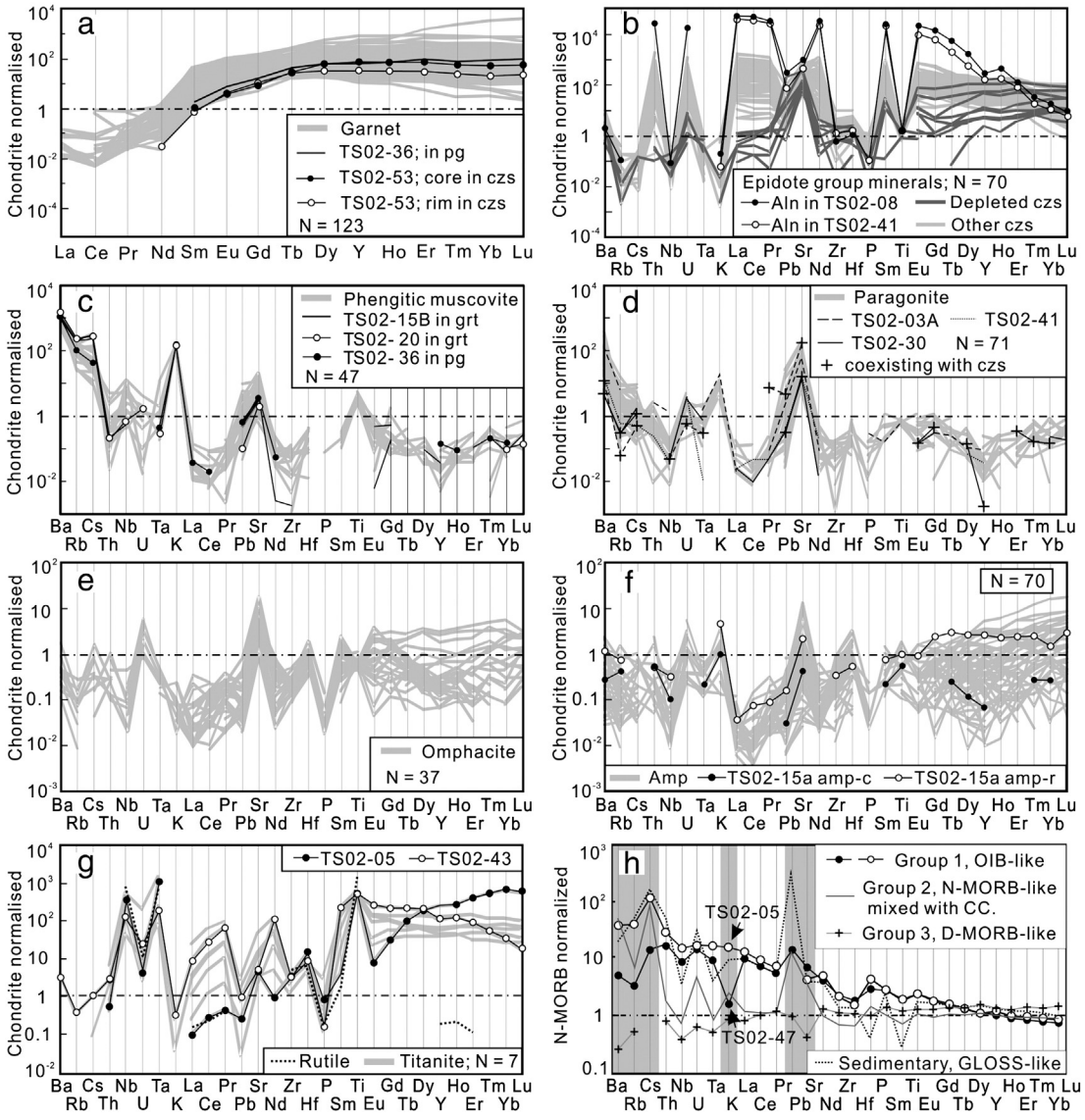

Fig. 4. Chondrite normalized (Sun and McDonough, 1989) mineral trace element diagrams (a–g; see Tables DR4–9 for data) and N-MORB normalized (Sun and McDonough, 1989) bulk-rock trace element diagram for representative rocks with different protolith compositions (h; see data in Table DR2). (a) REEs and Y distribution of garnet (gray lines; Pm between Nd and Sm is omitted for clarity). Three black lines represent garnet inclusions. Among others, two black lines with solid and hollow circles respectively represent the core and the rim of a garnet inclusion preserved in clinozoisite porphyroblast from TS02-53. (b) Different groups of epidote group minerals; the extremely enriched group (two black lines with circles); the depleted group (dark gray lines); and the others (light gray lines). (c) Phengitic muscovite (gray lines). Phengitic muscovite inclusions in garnet and paragonite have been highlighted. (d) Paragonite (gray lines). Paragonite inclusions in garnet have been highlighted. Compared with phengitic muscovite, paragonite shows lower LILEs and K but higher Sr and Pb. (e) Omphacite (gray lines). (f) Amphiboles (gray lines). Both the core (amp-c) and the rim (amp-r) compositions for one amphibole grain from TS02-15A have been highlighted for comparison. The (sodic–)calcic rim displays higher HREEs than the sodic amphibole core, probably resulting from the breakdown of garnet during late retrograde metamorphism. (g) Rutile (the dotted black curve) and titanite (gray lines). Two titanite grains discussed in details in the relevant text have been highlighted, *i.e.*, one titanite crystal with the highest HREEs in chlorite replacing garnet (from TS02-05), one titanite grain with high MREEs that has replaced epidote group minerals (from TS02-43). (h) N-MORB normalized trace element diagram of bulk-rock compositions for representative rocks of basaltic protoliths from different groups and of sedimentary protolith. Rock samples, TS02-05 and TS02-47 from Group 1, are also used for reconstruction of trace element budgets in Fig. 7. TS02-50B, TS02-17b and 986-1 are selected as the representative rocks of Group 2, Group 3 and meta-sedimentary rocks respectively. Elements plotted in light-gray areas are those considered as mobile elements discussed in Section 5.2 and in the study of Xiao et al. (2012). This is consistent with the highly variable content of these elements for rocks from a co-genetic group (*e.g.*, comparison between TS02-05 and TS02-47). GLOSS—global oceanic subducted sediments, Plank and Langmuir, 1998. D-MORB—depleted MORB.

stoichiometrically constrained in phengitic muscovite, but Ba, Rb and Cs are not, even though they occupy the K lattice site. No inter-LILE correlations exist, except for a good correlation between Rb and Cs (Fig. 5b,d).

The LILE contents in phengitic muscovite crystals of the same generation within a rock of basaltic protolith are constant, but their contents in phengitic muscovite crystals from different rocks of basaltic protoliths, especially those from different groups, are relatively variable (Table DR6 and Fig. 5a,b). This may reflect the effect of compositional inheritance from their protoliths. However, almost all data points representing the phengitic muscovite grains from rocks of basaltic protoliths cluster together in the Ba–Rb–Cs variation diagrams, with several "exotic" data points in Fig. 5a,b. White mica grains from the same rock plot both in the data cluster and as exotic data points, which cannot be caused by the compositional inheritance. The detailed petrography shows that the most scattered data points within a rock represent retrograde phengitic muscovite crystals. For example, one phengitic muscovite grain replacing the rim of garnet from TS02-15B contains higher Ba, Rb and Cs than two inclusions from the same sample (Fig. 5a,b), although phengitic muscovite inclusions from TS02-15B also show high contents of these elements (Figs. 4c, 5a,b; see data in Table DR6). This may indicate stronger effect of alteration at different stages of the SZM than the protolith inheritance.

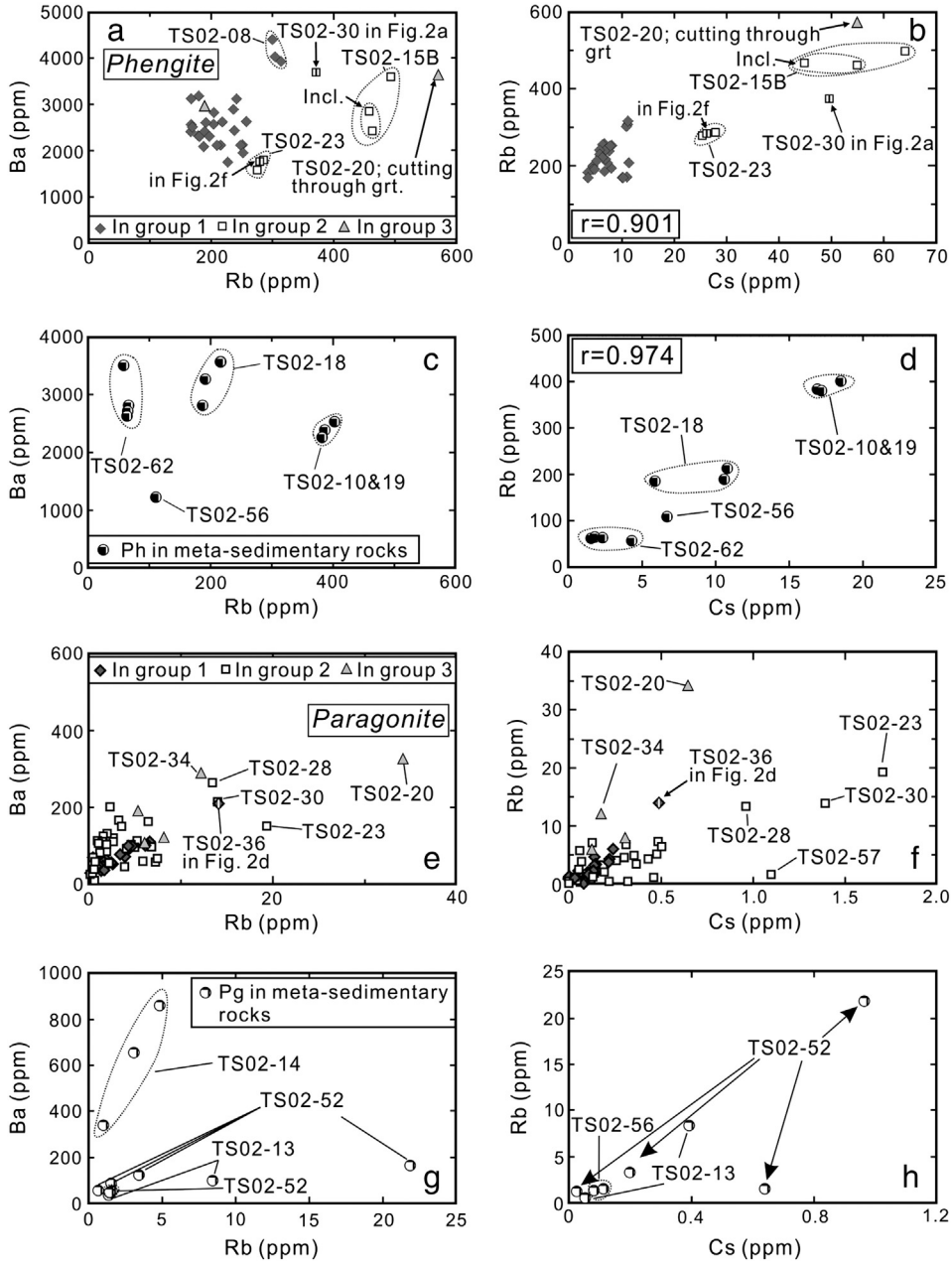

Fig. 5. Co-variation diagrams of K–Rb–Cs–Ba for both phengitic muscovite (a–d) and paragonite (e–h). (a)–(b) and (e)–(f) are for rocks of basaltic protolith from different groups, and (c)–(d) and (g)–(h) are for rocks of sedimentary protolith. The scattered points have been specifically labeled. The labeled points with a vertical bar inside represent grains that have also been shown in Fig. 2.

In rocks of sedimentary protolith, although no phengitic muscovite of different generations can be identified petrographically, the abundances of Ba, Rb and Cs in phengitic muscovite are more variable within each sample (Fig. 5c,d) than is the case for rocks of basaltic protolith (Fig. 5a,b), which may indicate stronger protolith control and less later SZM effects (Fig. 5c,d). Contents of Li, Sr, and importantly Pb, are also generally higher in phengitic muscovite from rocks of sedimentary protolith than in those of basaltic protolith (Fig. 6a and Table DR6).

4.2.2.2. Paragonite. Paragonite has 10–100 times chondrite values for LILEs (Fig. 4d), and contains up to an order of magnitude higher Sr relative to phengitic muscovite (Fig. 6a and Table DR6). Except for TS02-14, all the other paragonite crystals from rocks of both sedimentary and basaltic protoliths exhibit good correlations of K with Ba and Rb (not shown).

The paragonite coexisting with clinozoisite as inclusions in garnet (*e.g.*, TS02-03A, TS02-30, TS02-41) shows lower Ba, Rb, Cs (except one from TS02-03A), and, to a lesser extent, Pb and Sr than other paragonite grains from the same rock (Fig. 4d and Table DR6). Like the case for phengitic muscovite in rocks of basaltic protolith, the "exotic" data points in Fig. 5e,f represent the retrograde paragonite (*e.g.*, one replacing the rim of garnet or one even including a garnet relict, Fig. 2d), which shows generally higher Ba, Cs and Rb than other paragonite grains within the same rock. The difference of these scattered points with the Ba–Rb–Cs data cluster for paragonite in rocks of basaltic protolith thus may also suggest strong controls of alteration at different stages of the SZM on these elements in addition to compositional inheritance from their protoliths.

Paragonite from rocks of sedimentary protolith contains higher Pb and Sr than those from rocks of basaltic protolith (Fig. 6a). A stronger protolith control on Ba, Cs and Rb is also apparent for

paragonite from meta-sediments (Fig. 5g,h) as is the case for phengitic muscovite.

4.2.3. Epidote group minerals

Compared with other minerals, epidote group minerals, especially allanite, have the highest Th, U and LREEs (Fig. 4b; up to ~1000 ppm, 100s ppm and 10^5 ppm respectively in allanite, *e.g.*, Table DR5). HREEs, Sr and Pb are also highly enriched, up to 100–1000 times chondrite values (Fig. 4b). The abundances of all these elements, especially LREEs, are highly variable (Fig. 4b), within or between different rocks, or even between different parts of a single epidote grain (shown as the compositional zoning of epidote, *e.g.*, Fig. 6b). Three groups can be distinguished roughly in terms of the extent of LREE enrichments: the extremely enriched group, *i.e.*, allanite (one inclusion in garnet from TS02-08 and the core of a single grain in the omphacitic matrix of TS02-41); the extremely depleted group (TS02-13; TS02-16; TS02-62; one in TS02-43; one in TS02-52; one in TS02-54); and the rest. The large compositional variability may result from several factors, including variable bulk-rock compositions of the protolith rocks (no depleted epidote crystal is from rocks of Group 1 with OIB-like protolith; see Table DR5), the competition of coexisting minerals and the possibly large variation range in mineral-fluid partition coefficients of REEs for epidote group minerals (which is temperature dependent; Brunsmann et al., 2001; Feineman et al., 2007; Martin et al., 2011).

(Clino)zoisite inclusions, which coexist with paragonite in garnet, generally show low Sr and Pb, compared with the matrix (clino)zoisite from the same rock (*e.g.*, TS02-30 in Table DR5). In addition, the significant Th–U correlation in epidote group minerals (Fig. 6d) may account for the significant correlation between Th and U in bulk rocks, *i.e.*, $r = 0.968$ for epidote group minerals ($N = 68$) *vs.* $r = 0.9516$ for bulk rocks ($N = 48$) at >99% confidence levels.

4.2.4. Rutile and titanite

Because of the small grain size, we were only able to obtain reliable analytical data for one rutile grain in this study. It contains the highest Nb and Ta (among all the analyzed minerals, ~10^3 times chondritic values), and Zr and Hf (Table DR7), but relatively lower REEs than titanite (Fig. 4g). The concentrations of HFSEs in titanite are commonly less than those in rutile (Table DR7). The content of Sr in titanite can be up to 100 times the chondritic value (Fig. 4g). As the third important host for Pb and Sr (following epidote group minerals and white micas), titanite also shows a significant Pb–Sr correlation ($r = 0.950$ for $N = 7$, Fig. 6f). It generally shows high HREEs or slightly convex-up ($MREE_N > HREE_N$) patterns (*e.g.*, comparison between two highlighted titanite samples in Fig. 4g). LREEs in titanite vary from 100 times the chondritic value to somewhat depleted values (Fig. 4g). The variability of REEs in titanite is spatially controlled by surrounding minerals, at the expense of which the titanite has grown or recrystallized. Specifically, a retrograde titanite grain with a good prismatic shape, together with chlorite, has replaced the rim of a HREE-rich garnet porphyroblast (Fig. 2h). As a result, this titanite is characterized by very high HREEs (comparable or even higher than those in the related garnet), but relatively low LREEs (from TS02-05 highlighted in Fig. 4g; also see data in Table DR7). However, one titanite grain replacing a MREE-rich clinozoisite shows a slightly convex-up pattern (from TS02-43 highlighted in Fig. 4g).

4.2.5. Omphacite; glaucophane and other amphiboles

Omphacite contains high Li (10s of ppm; see Table DR8) as reported previously (*e.g.*, John et al., 2008). It also contains high Sr (Fig. 4e), up to 135 ppm (Table DR8). Glaucophane is essentially barren in terms of incompatible elements with only a few elements reaching ppm levels; Li is up to tens of ppm (Table DR9). It is notable that the late-formed (sodic–)calcic amphibole shows generally higher LILEs, Sr, Pb and HREEs than the early-formed Na-amphibole (Table DR9 and Fig. 4f), as clearly shown by those with growth zonings (*e.g.*, Fig. 2g). HFSE contents are low in both amphibole and omphacite, and Ta is often below the detection limit (Tables DR8–9).

4.2.6. Other minerals

Several grains of albite (Table DR8) and chlorite (Table DR9) were also analyzed. Except for Sr and Ba in albite (100s and 10s of ppm, respectively) and Li in chlorite (10s ppm), these two minerals contain low concentrations of all the other analyzed incompatible trace elements, showing their poor hosting capacity.

Because no lawsonite was found (only lawsonite pseudomorphs, replaced by clinozoisite and paragonite), and apatite and zircon are either too small or too rare to be identified petrographically, these minerals were not analyzed in this study.

5. Discussion

5.1. Trace element budgets in UHP metamorphic rocks

Based on the analyzed mineral trace element concentrations and mineral modal abundances through point counting, we reconstructed the trace element budgets for two representative metamorphic rocks of basaltic protoliths in Fig. 7 (TS02-05, a retrograde epidote blueschist and TS02-47, a highly eclogitic omphacitite from Group 1). Although large uncertainties exist as a result of mineral compositional variability in a given rock and unanalyzed accessory minerals like zircon and apatite, most of the trace element budgets in Fig. 7 are reasonably well constrained. Reconstructed HFSEs are poorly constrained and not shown in Fig. 7. The poor constraint on Zr and Hf is likely due to zircons that are unanalyzed, and the poor constraint on Nb and Ta is caused by less reliable analytical data for rutile with too small size for analysis.

Garnet is the main host for HREEs. Phengitic muscovite and paragonite essentially accommodate all of the Ba, Rb and Cs; the former hosting the majority of these elements (*e.g.*, Fig. 7a). Paragonite can also host a significant portion of Sr and Pb (Fig. 7a). Epidote group minerals contain more than 95% of LREEs, Th, U, Pb and Sr, around 60% of MREEs and less than 30% of HREEs in the bulk rock. Concentrations of Pb and Sr in clinozoisite are respectively ~20 times and ~4 times those in the coexisting paragonite in equilibrium (Fig. 6g,h), supported by the coexisting paragonite and clinozoisite in the form of lawsonite pseudomorphs in garnet porphyroblast (*e.g.*, Fig. 2a). Titanite can also accommodate some REEs, Sr and Pb, especially HREEs, *e.g.*, up to 30% in retrograde titanite that replaced rims of garnet (Figs. 2h, 7b). Although omphacite and amphibole can volumetrically constitute a large proportion of mineral assemblages, they contribute little to the bulk-rock trace element budgets owing to their very low contents of all the trace elements but Li and Be (not shown in Fig. 7).

5.2. Elemental responses to SZM

5.2.1. Mobility/immobility and variations of K, Ba, Rb and Cs

The K and Na abundances in the protolith governed the presence and amount of phengitic muscovite and paragonite respectively in metamorphic rocks we studied, but concentrations of Ba, Rb and Cs in the protolith can also affect the concentrations of these elements in white micas. However, once elements are stabilized in the mineral host, the relevant mineral trace element content and the mineral modal abundance determine the bulk-rock abundances of these elements in metamorphic rocks as shown in Fig. 7. Therefore, K, Ba, Rb and Cs in white micas largely account for their bulk-rock abundances.

The petrography suggests that the compositional differences of white mica grains within a rock of basaltic protolith may reflect their formation at different metamorphic stages (*e.g.*, white micas with exotic compositions are of retrograde origin). That is, the Ba–Rb–Cs contents of white micas within a metamorphic rock of basaltic protoliths are not only controlled by the protolith composition, but also by fluid compositional changes during the SZM.

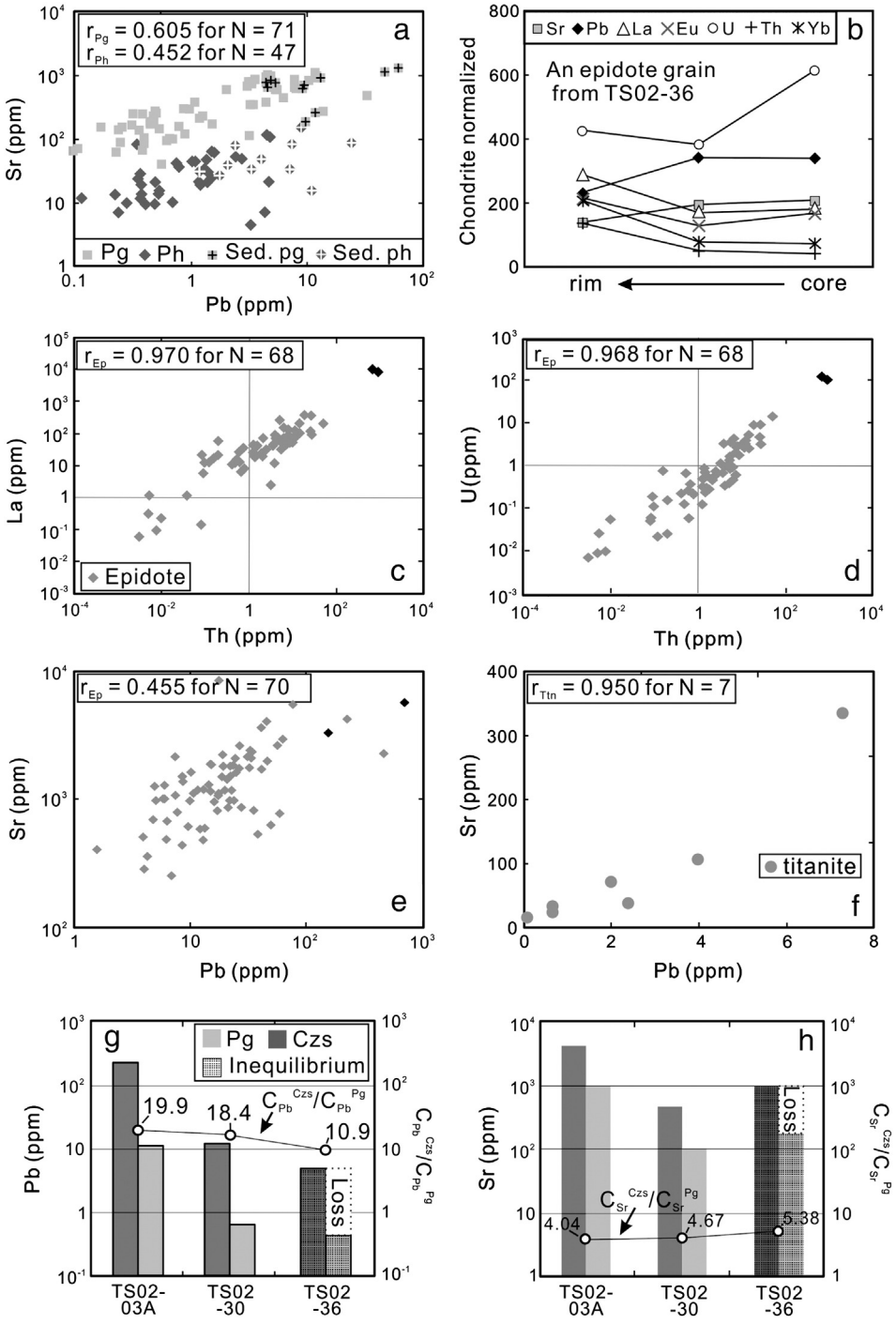

Fig. 6. (a) Co-variation diagram of Pb and Sr for both paragonite and phengitic muscovite. Sed.—sedimentary protolith. The markers with cross inside represent micas from rocks of sedimentary protolith. Both paragonite and phengitic muscovite from rocks of sedimentary protolith have higher Pb and Sr than those from rocks of basaltic protolith. The high Pb and Sr contents of paragonite could even be comparable to those of epidote group minerals in Fig. 6e. (b) Profile of selected trace element contents for one epidote grain from TS02-36 (see data in Table DR5). Different multiplication factors have been given for different elements: (Sr, Th, La, Eu) × 1; (U, Yb) × 10; Pb × 100. It shows a rim-ward increase of REEs and Th but decrease of Pb and Sr. (c–e) Co-variation diagrams of La, Th, U, Pb and Sr for epidote group minerals (including two highlighted allanite grains). (f) Correlation diagram of Pb–Sr for titanite. (g–h) Histograms of Pb and Sr contents for pairs of paragonite and clinozoisite. The first two pairs of columns in each panel represent Pb and Sr contents of coexisting paragonite and clinozoisite inclusions in garnet porphyroblasts, *i.e.*, lawsonite pseudomorphs. The content ratios of Pb and Sr in these two neighboring minerals (*i.e.*, C_{Pb}^{Ep}/C_{Pb}^{Pg} and C_{Sr}^{Ep}/C_{Sr}^{Pg}, the right vertical axis) can be used to infer the partition coefficient between these two minerals in equilibrium, represented by the circles; ~20 and ~4 for $Kd_{Pb}^{Czs/Pg}$ and $Kd_{Sr}^{Czs/Pg}$ respectively. One paragonite porphyroblast and its clinozoisite relict inclusion from TS02-36 are also plotted, as the last pair of columns and labeled as 'inequilibrium'. The blank areas constrained by the dotted edges represent the loss of Pb and Sr with the clinozoisite–paragonite transition.

Based on detailed petrography, we can classify white micas in rocks of basaltic protoliths into three generations: generation 1 of white micas (G I) is represented by inclusions in garnet produced during the early prograde metamorphism; generation 2 of white micas (G II) are those crystals preserved in the omphacite matrix that may be equilibrated under late stage prograde metamorphic conditions; generation 3 of white micas (G III) is of retrograde origin. To properly evaluate the effect of metamorphism on mineral compositions, we need to isolate the effect of protolith control. For this, we choose several paragonite crystals of the three generations from one sample (TS02-30; see data in

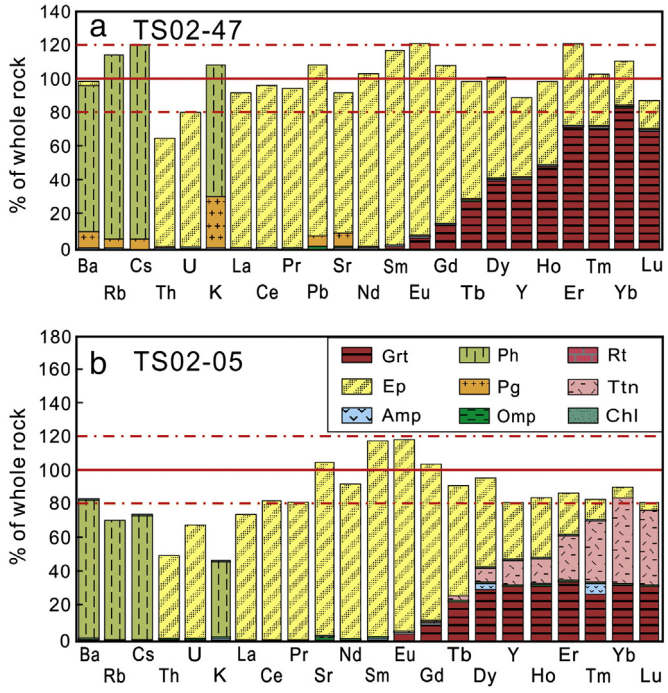

Fig. 7. Reconstructed trace element budgets normalized by the analyzed bulk-rock composition for representative rocks of basaltic protoliths, *i.e.*, TS02-47 (omphacitite) and TS02-05 (retrograde epidote blueschist). The analyzed bulk-rock compositions of these two rock samples can be referred to Fig. 4h and Table DR2. Two red dot-dashed lines in each panel represent the deviation of our reconstructed bulk-rock composition from the analyzed composition with ±20%. In (b), Pb is not reconstructed because of the unavailable analyzed Pb content for TS02-05. (For interpretation of the references to color in this figure legend, the reader is referred to the web version of this article.)

Table DR6). These include those coexisting with clinozoisite as inclusions in garnet (G I; Fig. 2a), a single relict with a reaction rim in the omphacite matrix (G II) and a retrograde mica replacing the rim of garnet (G III).

The contents of Ba, Rb, Cs, Pb and Sr in G II are higher than those in G I, which are probably inherited from their precursor minerals like lawsonite with very low contents of Ba, Rb and Cs (*e.g.*, Gao et al., 1999; Xiao et al., 2013). Meanwhile, because REEs, Pb and Sr in the prior lawsonite would be preferentially incorporated into the newly-formed clinozoisite relative to paragonite (*i.e.*, $[Czs/Pg]_{Pb} = 20$ and $[Czs/Pg]_{Sr} = 4$; Fig. 6g,h), even lower Pb and Sr are found in the neighboring paragonite inclusions.

The retrograde paragonite (G III) has the highest Ba, Rb and Cs among all the analyzed paragonite grains from TS02-30 (forming one of the exotic points in Fig. 5e,f). This significant re-enrichment effect can also be observed in other micas, *e.g.*, one retrograde phengitic muscovite (G III) from TS02-15B shows much higher Ba and Cs contents than two phengitic muscovite inclusions (G I) from the same sample (Fig. 5a,b). Considering these white mica grains are within one rock, these compositional variations are thus protolith independent. The observation that the scattered points in Fig. 5a,b,e,f represent retrograde white micas may imply that the re-enrichment process happened during the retrograde metamorphism (also see Lü et al., 2012 for other evidence of this re-enrichment for UHP eclogites from Western Tianshan). The fluids released from the subducted oceanic crust during the eclogitization or from the underlying serpentinized lithosphere will move upwards (because of their low density), and rehydrate metamorphic rocks at shallower levels (Xiao et al., 2012). Along with the migration of these released fluids, LILEs will also be transported and incorporated into newly-formed minerals, especially new generations of white micas. However, further analysis for different generations of white micas should be done to test this interpretation/hypothesis.

Therefore, the Ba–Rb–Cs contents of white micas within a metamorphic rock of basaltic protolith are affected by the alteration during the SZM as well as by the inheritance of Ba–Rb–Cs from the protolith. This alteration of Ba–Rb–Cs contents at different stages of the SZM may indicate the mobility of these elements. In comparison, although Ba–Rb–Cs contents are more variable in white micas from rocks of sedimentary protoliths, the lack of exotic data points within the rock may suggest that the variation of these elements is inherited from their protolith compositions or resulted from a small scale redistribution, indicating the immobility of these elements in rocks of sedimentary protolith. By examining correlations among incompatible elements in bulk-rock compositions, Ba, Cs and Rb show different relationships with HFSEs in different lithologies (poor in meta-basalts *vs.* good in meta-sediments). This also indicates different responses of these elements to the SZM in different lithologies on the basis of bulk-rock compositional studies for the same rocks (mobile in rocks of basaltic protolith *vs.* immobile in rocks of sedimentary protolith) (Xiao et al., 2012). Furthermore, by comparing rocks of basaltic protolith from the same group, the depletion of Ba–Rb–Cs in eclogites with less retrograde overprints (*e.g.*, TS02-03B, TS02-47) and the enrichment of these elements in the highly retrograde blueschists (*e.g.*, TS02-03A, TS02-05) indicate the loss during prograde metamorphism but the gain during retrograde metamorphism (see data in Table DR2 and Fig. 4h for comparison; Xiao et al., 2012). This implies the mobility of Ba–Rb–Cs during both prograde and retrograde metamorphism in rocks of basaltic protoliths.

As mentioned in Section 4.2.5, the late-formed (sodic–)calcic amphibole also shows generally higher Ba, Cs, Rb, Sr and Pb than the early-formed Na-amphibole (Table DR9 and Fig. 4f), clearly evidenced by the amphibole with growth zonings (*e.g.*, Fig. 2g). Considering that retrograde white micas also show higher contents of Ba–Rb–Cs than do prograde ones, the higher contents of Ba–Rb–Cs, Sr and Pb in the late-formed (sodic–)calcic amphibole may be also attributed to the mobility of these elements in response to the infiltration of external fluids.

5.2.2. Geochemical behaviors of other key trace elements

As shown above (also Figs. 4b & 7), most of the LREEs, Th and U, and some Pb and Sr are hosted in epidote group minerals, which accordingly control the budget of these elements in the bulk rock. The stability of epidote group minerals thus affects the behavior of these elements during the SZM. However, the significant inter-correlations of LREEs, Th, and U (Fig. 6c,d) but the poor correlations of these elements with Sr or Pb (not shown) in epidote group minerals suggests that the behavior of LREEs, Th and U is decoupled from that of Pb and Sr during the SZM.

During the SZM, because lawsonite, epidote group minerals, garnet, titanite and rutile are stable over a large *P–T* range (Fig. 3), REEs, Th, U and HFSEs hosted by these minerals could be exchanged among these minerals and largely redistributed into the newly-formed minerals without significant loss from the system, resulting in their overall immobility throughout the SZM. In contrast, although epidote group minerals can contain high Pb and Sr contents (paragonite to a lesser extent; *e.g.*, Fig. 7a), the low partition coefficient of Sr between lawsonite and fluids reported recently (Martin et al., 2011) may explain that some Sr may leave to the fluids that are in equilibrium with lawsonite. In addition, on the basis of estimated bulk partition coefficients for the reaction products, Feineman et al. (2007) calculated the composition of the fluids produced through specific dehydration reactions related to the breakdown of (clino)zoisite. The calculated fluids show consistently high Pb and Sr but variable LREE contents (Feineman et al., 2007). Take one of the main reactions during the blueschist-to-eclogite transition: 13 Gln + 6 Czs = 9 Prp + 26 Jd + 12 Di + 19 Coe/Qz + 16 H_2O as an example (Reaction 3 in Feineman et al., 2007), the calculated bulk partition coefficients of Pb and Sr for the reaction products (Grt + Cpx + Qz) are much lower (*i.e.*, 0.01 and 0.3 respectively) than those of LREEs (*e.g.*, 6 for La, 15 for Ce) (Feineman et al., 2007). This indicates that Pb and Sr are mobile relative to LREEs during this dehydration. The mobility of Pb and Sr but the immobility of REEs,

Th and U is also consistent with our previous conclusion based on bulk-rock study for the same rocks (Xiao et al., 2012). The mobilized Pb and Sr are then carried by the released fluids, which are manifested by dehydration veins (John et al., 2008), and may further play a role in the enrichment of these elements in arc lavas.

5.3. Elemental (re-)distributions during subduction-zone metamorphism

The trace element budgets are controlled by key minerals in which these elements are hosted, which in turn depend on the protolith compositions, metamorphic conditions (pressure, temperature, fluids) and the SZM history. The trace element (re-)distributions in response to the SZM, as illustrated in Fig. 8, are discussed in this context as follows.

5.3.1. Constraints on prograde and peak metamorphism ($P < 3$ GPa)

We can summarize that under blueschist facies metamorphic conditions, the significant mineral phases for hosting incompatible trace elements are phengitic muscovite (LILEs, and some Sr and Pb), titanite (HFSEs, REEs, and, Pb and Sr to a lesser extent), and epidote group minerals (REEs, Th, U, Pb and Sr). In our recent work on metamorphic rocks from North Qilian Mountain, a high pressure (HP) metamorphic belt in NW China (Xiao et al., 2013), lawsonite was also reported as an important host for REEs, U, and Th in the blueschist facies. Although lawsonite was not found, the presence of lawsonite pseudomorphs (replaced by paragonite and clinozoisite) in the core–mantle portions of garnet porphyroblasts in our samples from Western Tianshan indicates previous occurrence of lawsonite during the early stage of the SZM. The prior lawsonite thus should be of significance for the trace element budget for rocks from Western Tianshan.

With the eclogitization (stage 1, *i.e.*, prograde blueschist facies in Fig. 8a), significant amounts of H_2O would be released during the transition from blueschist to eclogite facies (*e.g.*, Pawley and Holloway, 1993; Poli and Schmidt, 2002). As we have mentioned in Section 5.2.2, because of the low bulk rock–fluid partition coefficient of Pb and Sr for the specific dehydration reactions related to the breakdown of (clino) zoisite (Feineman et al., 2007), some Pb and Sr would be liberated into fluids and display their mobility (decoupled from LREEs), reflected by the loss in Fig. 8a. However, the REEs previously hosted in epidote group minerals will be redistributed into newly formed allanite and garnet (the dominant host for HREEs subsequently). Phengitic muscovite, together with paragonite, when formed will incorporate almost all the Ba, Cs and Rb (although some of these elements could be lost prior to the formation of white micas and display their mobility, shown as the loss in Fig. 8a). Additionally, titanite may become unstable and replaced by rutile at this stage, through which REEs are transferred into newly-formed garnet and allanite, while Nb and Ta are entirely redistributed into rutile. Although Gao et al. (1999), Gao and Klemd (2003) and Spandler et al. (2003) suggested that lawsonite may also have broken down at this stage, trace elements hosted in the prior lawsonite would largely, if not entirely, be conserved by newly-formed epidote group minerals (*e.g.*, allanite) and garnet.

Up to the peak metamorphic condition (stage 2, UHP eclogite facies in Fig. 8b), a large proportion of REEs has been accumulated and sequestered in already produced lawsonite, epidote group minerals and garnet, and thus less REEs can be supplied to the late-formed relevant minerals, typically reflected by a general rim-ward decrease of HREEs in garnet (Fig. 4a; also King et al., 2004; Bebout, 2007; John et al., 2008; El Korh et al., 2009). As phengite could be stable even up to 10 GPa (~300 km; *e.g.*, Sorensen et al., 1997), those LILEs hosted in phengitic muscovite formed during prograde metamorphism would be entirely carried by this phase into the deep mantle.

5.3.2. Constraints on retrograde metamorphism

During retrograde metamorphism, amphiboles (mostly [sodic–] calcic amphibole with some glaucophane), epidote group minerals and chlorite replaced garnet, omphacite and lawsonite (stages 3 and 4, retrograde eclogite facies and epidote amphibolite facies in Fig. 8c and d). The occurrence of retrograde white micas reflects the rehydration during retrograde metamorphism. The commonly higher Ba, Rb and Cs contents in retrograde white micas (*e.g.*, Fig. 5a,b,e,f) indicate that re-enrichment resulted from rehydration, which is also reflected by the enriched bulk-rock composition of retrograde metamorphic rocks, shown as the gain in Fig. 8c,d (*e.g.*, enriched retrograde metamorphic rock TS02-05 *vs.* depleted eclogite TS02-47 in Fig. 4h; also see Xiao et al., 2012). Pb and Sr may also have been re-enriched by rehydration. Retrograde epidote group minerals recrystallized at this stage. However, they may contain lower REE contents when all the lawsonite has reacted out, because less REEs are available as they have been largely stored in the epidote group minerals already present (although some more HREEs could be provided during the breakdown of garnet). Meanwhile, rutile was replaced by titanite, through which Ti, Nb and Ta would be transferred back to titanite again (also see Lucassen et al., 2010, 2011). Owing to the further breakdown of garnet (stage 4 and afterwards), HREEs would be largely taken up by the newly-formed retrograde titanite. For example, the titanite grains from TS02-05, together with chlorite, have replaced garnet (Fig. 2h), and their HREE contents (Fig. 4g) are even higher than those in the garnet they are replacing. The relatively higher HREEs in the retrograde (sodic-)calcic amphiboles compared with the prograde glaucophane (Fig. 4f and Table DR9) may also be due to the breakdown of garnet, the most important HREE host.

6. Implications

6.1. On the geochemistry of arc lavas

Arc lavas have been widely accepted to be produced by slab-dehydration induced mantle wedge melting, which gives the typical arc signatures (enriched in Ba, Cs, Rb, Pb, Sr, U, Th and LREEs while depleted in HFSEs). Eclogites from Western Tianshan are considered to have experienced >2.5 GPa SZM evidenced by the occurrence of coesite (Lü et al., 2008, 2009). Even though no coesite has been found in our eclogitic samples, they were collected from the same locations with the same mineral assemblages, and thus most probably experienced the same metamorphic conditions. Therefore, they can be used to evaluate the geochemical consequences of subduction-zone metamorphism at depths greater than 75 km (see details in Xiao et al., 2012). The enrichment of Ba, Cs, Rb, Pb and Sr in arc lavas is apparently consistent with the relative mobility of these elements during the SZM as discussed above (also see Xiao et al., 2013). The geochemical behavior of LREEs during the SZM is controversial; they are claimed as immobile by many (*e.g.*, Kogiso et al., 1997; Usui et al., 2007) and mobile by others (*e.g.*, Brunsmann et al., 2000, 2001; John et al., 2004). Their different behaviors are mainly attributed to different mechanisms of fluid transport, *i.e.*, channelized fluids may lead to the mobility of LREEs, especially if large amounts of fluids are present (*e.g.*, John et al., 2008). In our study, because of the strong capability of epidote group minerals to house LREEs, Th and U (their main host), and the large stability fields of the minerals that host these elements (*i.e.*, lawsonite, titanite, epidote group minerals), we have shown that metamorphic dehydration of the subducting altered ocean crust most likely has not contributed to the enrichment of LREEs, Th or U in subduction-zone magmatism up to 75 km depth.

These observations are important because it simply means that the standard "flux-melting" (simple slab-dehydration induced mantle wedge melting) may not be an effective means of producing arc magmatism (also see Xiao et al., 2012, 2013). A recent experimental study (Schmidt et al., 2004) shows that phengite could be dissolved in a supercritical fluid beyond the second critical endpoint (5–6 GPa for K-/mica-rich lithologies of the subducted oceanic crust in Schmidt et al., 2004). Therefore, the supercritical fluids may carry phengite-hosted elements (*e.g.*, K, Ba, Cs and Rb) to metasomatize the overlying mantle wedge, and lead to further partial melting enriched in these

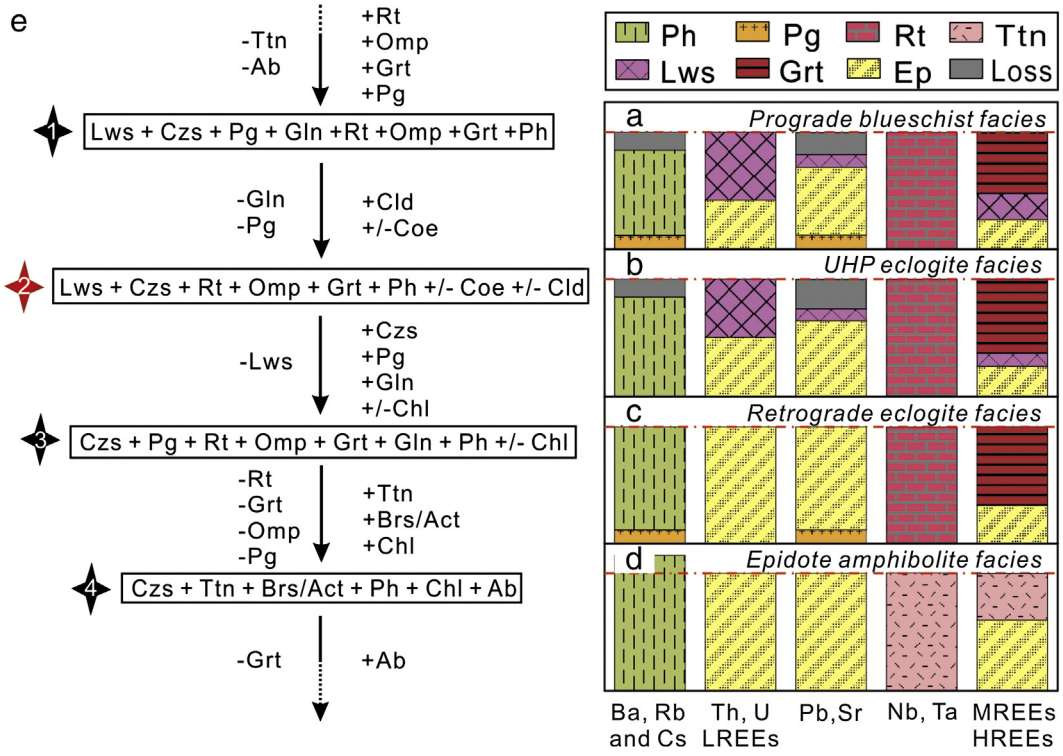

Fig. 8. Schematic diagrams of element redistributions for rocks of basaltic protoliths (a–d) in response to the four stages of SZM given in Fig. 3, along with the sequence of different mineral appearance and disappearance (e). The red dot-dashed lines in (a)–(d) represent the assumed original bulk-rock composition before the SZM. (For interpretation of the references to color in this figure legend, the reader is referred to the web version of this article.)

elements. Meanwhile, based on experimental studies (Hermann, 2002), the dissolution of allanite (an important epidote group mineral for LREEs, Th and U) at higher temperatures (~900 °C and ~1000 °C for meta-basalts and meta-sediments respectively), could lead to the high solubility of LREEs in the coexisting liquid (fluids or melts). Therefore, slab contributions may actually take the form of hydrous melts (*e.g.*, Hermann and Rubatto, 2009) or supercritical fluids/transitional fluids (see definition in Schmidt et al., 2004; Hermann et al., 2006; Mibe et al., 2011) at higher temperatures and/or greater depths, under which conditions, LREEs, Th and U could be mobilized. Furthermore, in the standard slab-dehydration induced mantle wedge melting model, the enriched U and LREEs in arc lavas are considered as mobile elements by aqueous fluids, in which case, they are expected to have no correlations with immobile elements (*e.g.*, Nb). However, in Fig. 9, U and La of arc lavas show significant correlation with immobile Nb, which contradicts the standard slab-dehydration induced mantle wedge melting model. Therefore, the correlations in Fig. 9 may also indicate that the formation of arc lavas is induced by the involvement of supercritical fluids or hydrous melts derived from the subducting oceanic crust/sediments (Hermann et al., 2006; Hermann and Rubatto, 2009).

In addition, through a detailed discussion on the apparent immobility of U, which indicates the form of U^{4+} (Bailey and Vala Ragnarsdottir, 1994), it has been inferred that the redox condition in subduction zones may be more reduced (Lee et al., 2003, 2005; Song et al., 2009; Xiao et al., 2012) than previously thought (oxidized condition in subduction zones, *e.g.*, Wood et al., 1990; Brandon and Draper, 1996). In this study, we have shown that the immobility of U like Th and their significant linear correlations (Fig. 6d) are largely controlled by the presence of epidote group minerals (to a lesser extent, maybe lawsonite, based on our recent studies on lawsonite-bearing blueschists from North Qilian Mountain in NW China; Xiao et al., 2013). This suggests that U may take its U^{4+} form to substitute in epidote group minerals. However, further studies are required to understand the redox conditions in subduction zones and the implications for geochemical behavior of U in this context.

6.2. On mantle compositional heterogeneity

After the SZM, mobile elements have been lost with the breakdown/dissolution of their host minerals (Schmidt, 1995), while the relatively immobile elements conserved in the stable minerals of the dehydrated oceanic crust can be carried into the deep mantle. These altered mobile elements and conservative immobile elements have direct bearing on the deep mantle compositional heterogeneity as interpreted by the

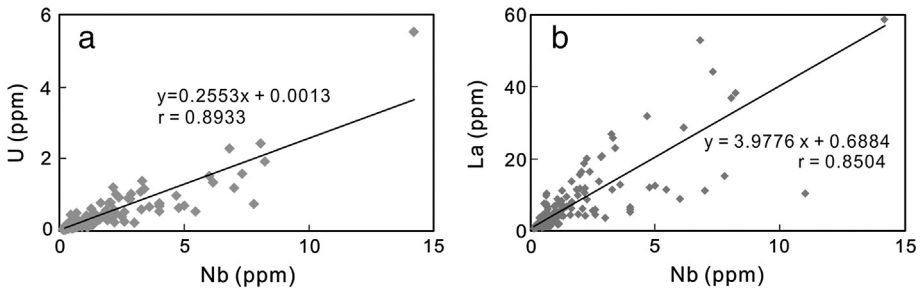

Fig. 9. Correlations of Nb with U and La observed in arc lavas (data referred to Elliott, 2003).

geochemical variability of oceanic basalts (*e.g.*, Weaver, 1991; Hofmann, 1997; Niu and O'Hara, 2003; Niu, 2004). Furthermore, if the element mobility is controlled by different minerals (*e.g.*, phengitic muscovite for Rb, clinozoisite for Sr) or the element changes are controlled by different processes during the SZM (*e.g.*, the involvement of supercritical fluids or hydrous melts for U, aqueous fluids for Pb), the ratios related to these elements in the residual subducted rocks passing through the SZM will determine the relevant elemental ratios in the deep mantle (*e.g.*, Rb/Sr, U/Pb), that cannot be the same as in rocks entering the trenches prior to the SZM.

Our previous study (*e.g.*, Xiao et al., 2013) and this work have revealed that REEs, Th and U are largely hosted in lawsonite, epidote group minerals and garnet (to a lesser extent, titanite), and Ba, Rb and Cs are hosted by white micas during the SZM. After the SZM, the Lu/Hf ratio in the residual subducted oceanic crust remains constant because Lu and Hf are both immobile, and should be largely conserved (Lu is largely in garnet, and Hf is largely in zircon and to a lesser extent in rutile). The Sm/Nd ratio could also be constant because Sm and Nd are hosted by the same minerals (*e.g.*, epidote group minerals, titanite) and thus have similar geochemical behaviors. However, the Rb/Sr ratio is significantly modified because it is affected by both white micas (for Rb) and epidote group minerals (for Sr), while the U/Pb ratio may also be changed significantly because U and Pb are mobilized through different mechanisms (aqueous fluids for Pb *vs.* supercritical fluids/melts for U). Therefore, alteration during the SZM will result in the absence of correlations between Rb/Sr (and possibly U/Pb) and Sm/Nd or Lu/Hf. Actually, poor correlations have been observed in the bulk-rock composition of these metamorphic rocks from Western Tianshan, *i.e.*, variable Rb/Sr (or U/Pb) ratios at constant Sm/Nd (or Lu/Hf) ratios in the representative residual subducted oceanic slab rocks (Xiao et al., 2012). These P/D ratios, with time, will result in similarly poor correlations between $^{87}Sr/^{86}Sr$ (or $^{206}Pb/^{204}Pb$) and $^{143}Nd/^{144}Nd$ or $^{176}Hf/^{177}Hf$ in the residual slab materials subducted into the deep mantle. Therefore, although AOC is expected to contribute to mantle compositional heterogeneity, it cannot be the major source material for oceanic basalts because subduction-zone-processed residual oceanic crust will result in Rb–Sr decoupling and hence Sr–Nd and Sr–Hf isotopic decoupling, which cannot explain the first order Sr–Nd–Hf isotope correlations defined by oceanic basalts, in particular OIB (Niu and O'Hara, 2003; Xiao et al., 2012).

7. Conclusions

Garnet, epidote group minerals, white micas, and Ti-bearing minerals are the most important minerals hosting incompatible elements in the subducting/subducted oceanic crust and sediments. Their presence and stability largely control the geochemical behaviors of chemical elements in response to the SZM. Different fluid properties (*e.g.*, aqueous fluids, supercritical fluids, hydrous melts) and resultant partitioning can also control elemental behaviors during the SZM. On the basis of our studies on bulk-rock compositions and mineral trace elemental data of the same metamorphic rocks from Western Tianshan, we further confirm that Ba, Rb, Cs, K, Pb and Sr are mobilized in meta-basaltic rocks, while only Pb and Sr are mobile in meta-sedimentary rocks with aqueous fluids (at depths in excess of 75 km in our studies); LREEs, Th and U can only be migrated in supercritical fluids or hydrous melts. Protolith composition, metamorphic conditions and metamorphic history, all together, control the mineral assemblages, the stability of these minerals, and hence the behaviors of chemical elements they host.

The common enrichments of U, Th and LREEs observed in arc magmas but the immobility of these elements during the dehydration of aqueous fluids indicate that hydrous melts generated at temperatures above the water-saturated solidus or supercritical/transitional fluids beyond the second critical endpoint are significant in generating "arc lava signatures". In addition, because elements such as LILEs and REEs are hosted in different mineral phases and/or because elements are released by different mechanisms, the AOC, after the SZM, cannot be responsible for the Sr–Nd (Hf) isotopic correlations observed in oceanic basalts and therefore cannot be the major source material for OIB.

Acknowledgments

The sampling conducted in 2002 was supported by a Natural Environment Research Council Senior Research Fellowship to Yaoling Niu, a NERC studentship to Shaun Lavis, and a Royal Society China joint project to Yaoling Niu, and also by the National Natural Science Foundation of China to Yaoling Niu (grant numbers: 9101400, 41130314) and the Chinese Geological Survey to Huaikun Li and Huichu Wang. Yuanyuan Xiao was supported by a Durham University Doctoral Fellowship. Thanks for the great help of Shan Gao, Ming Li, Keqing Zong and Shiwen Xie at the State Key Laboratory of Geological Processes and Mineral Resources, China University of Geosciences in Wuhan, and Honglin Yuan, Mengning Dai, Kaiyun Chen, and Guofen He at the State Key Laboratory of Continental Dynamics of Northwest University in Xi'an, China for using LA-ICPMS. Yongsheng Liu is acknowledged for supplying *ICPMSDATACAL* software. Shaun Lavis is very much thanked for his sampling. Comments from the associate editor (Laurie Reisberg) and reviewers (Jörg Hermann, Timm John, Lifei Zhang, Susanne Schmidt, and Afifé El Korh) have significantly helped to improve this paper and they are gratefully appreciated.

Appendix A. Supplementary data

Supplementary data to this article can be found online at http://dx.doi.org/10.1016/j.chemgeo.2013.12.005.

References

Ai, Y.L., Zhang, L.F., Li, X.P., Qu, J.F., 2006. Geochemical characteristics and tectonic implications of HP-UHP eclogites and blueschists in Southwestern Tianshan, China. Prog. Nat. Sci. 16 (6), 624–632.
Bailey, E.H., Vala Ragnarsdottir, K., 1994. Uranium and thorium solubilities in subduction zone fluids. Earth Planet. Sci. Lett. 124 (1–4), 119–129.
Bebout, G.E., 2007. Metamorphic chemical geodynamics of subduction zones. Earth Planet. Sci. Lett. 260, 373–393.
Becker, H., Jochum, K.P., Carlson, R.W., 2000. Trace element fractionation during dehydration of eclogites from high-pressure terranes and the implications for element fluxes in subduction zones. Chem. Geol. 163, 65–99.
Beinlich, A., Klemd, R., John, T., Gao, J., 2010. Trace-element mobilization during Ca-metasomatism along a major fluid conduit: eclogitization of blueschist as a consequence of fluid–rock interaction. Geochim. Cosmochim. Acta 74 (6), 1892–1922.
Brandon, A.D., Draper, D.S., 1996. Constraints on the origin of the oxidation state of mantle overlying subduction zones—an example from Simcoe, Washington, USA. Geochim. Cosmochim. Acta 60, 1739–1749.
Brunsmann, A., Franz, G., Erzinger, J., Landwehr, D., 2000. Zoisite- and clinozoisite-segregations in metabasites (Tauern Window, Austria) as evidence for high-pressure fluid–rock interaction. J. Metamorph. Geol. 18, 1–21.
Brunsmann, A., Franz, G., Erzinger, J., 2001. REE mobilization during small-scale high-pressure fluid–rock interaction and zoisite/fluid partitioning of La to Eu. Geochim. Cosmochim. Acta 65 (4), 559–570.
Carlson, W.D., 2002. Scales of disequilibrium and rates of equilibration during metamorphism. Am. Mineral. 87, 185–204.
Deer, W.A., Howie, R.A., Zussman, J., 1992. An Introduction to the Rock-Forming Minerals. Prentice Hall.
El Korh, A., Schmidt, S.T., Ulianov, A., Potel, S., 2009. Trace element partitioning in HP-LT metamorphic assemblages during subduction-related metamorphism, Ile de Groix, France: a detailed LA-ICPMS study. J. Petrol. 50, 1107–1148.
Elliott, T., 2003. Tracers of the slab. Geophys. Monogr. 138, 23–45.
Feineman, M.D., Ryerson, F.J., DePaolo, D.J., Plank, T., 2007. Zoisite-aqueous fluid trace element partitioning with implications for subduction zone fluid composition. Chem. Geol. 239, 250–265.
Gao, J., Klemd, R., 2003. Formation of HP-LT rocks and their tectonic implications in the western Tianshan Orogen, NW China: geochemical and age constraints. Lithos 66, 1–22.
Gao, J., Klemd, R., Zhang, L., Wang, Z., Xiao, X., 1999. *P–T* path of high-pressure/low-temperature rocks and tectonic implications in the western Tianshan Mountains, NW China. J. Metamorph. Geol. 17, 621–636.
Guillong, M., Hametner, K., Reusser, E., Wilson, S.A., Gunther, D., 2005. Preliminary characterisation of new glass reference materials (GSA-1G, GSC-1G, GSD-1G and GSE-1G) by laser ablation-inductively coupled plasma-mass spectrometry using 193 nm, 213 nm and 266 nm wavelengths. Geostand. Geoanal. Res. 29 (3), 315–331.

Hermann, J., 2002. Allanite: thorium and light rare earth element carrier in subducted crust. Chem. Geol. 192, 289–306.
Hermann, J., Rubatto, D., 2009. Accessory phase control on the trace element signature of sediment melts in subduction zones. Chem. Geol. 265 (3–4), 512–526.
Hermann, J., Spandler, C., Hack, A., Korsakov, A.V., 2006. Aqueous fluids and hydrous melts in high-pressure and ultra-high pressure rocks: implications for element transfer in subduction zones. Lithos 92, 399–417.
Hernandez, S.Y., 2001. Petrologic and chemical examination of the blueschists of Syros, Greece. http://www.science.smith.edu/departments/Geology/Greece/Abstracts/Hernandez.pdf.
Hofmann, A.W., 1997. Mantle geochemistry: the message from oceanic volcanism. Nature 385 (16), 219–229.
Hofmann, A.W., White, W.M., 1982. Mantle plumes from ancient oceanic crust. Earth Planet. Sci. Lett. 57, 421–436.
Jochum, K.P., Willbold, M., Raczek, I., Stoll, B., Herwig, K., 2005. Chemical characterisation of the USGS reference glasses GSA-1G, GSC-1G, GSD-1G, GSE-1G, BCR-2G, BHVO-2G and BIR-1G using EPMA, ID-TIMS, ID-ICP-MS and LA-ICP-MS. Geostand. Geoanal. Res. 29 (3), 285–302.
John, T., Scherer, E.E., Haase, K., Schenk, V., 2004. Trace element fractionation during fluid-induced eclogitization in a subducting slab: trace element and Lu–Hf–Sm–Nd isotope systematics. Earth Planet. Sci. Lett. 227, 441–456.
John, T., Klemd, R., Gao, J., Garbe-Schonberg, C.D., 2008. Trace-element mobilization in slabs due to non steady-state fluid–rock interaction: constraints from an eclogite-facies transport vein in blueschist (Tianshan, China). Lithos 103 (1–2), 1–24.
Kelley, K.A., Plank, T., Ludden, J., Staudigel, H., 2003. Composition of altered oceanic crust at ODP sites 801 and 1149. Geochem. Geophys. Geosyst. 4.
Kessel, R., Schmidt, M.W., Ulmer, P., Pettke, T., 2005. Trace element signature of subduction-zone fluids, melts and supercritical liquids at 120–180 km depth. Nature 437, 724–727.
King, R.L., Bebout, G.E., Kobayashi, K., Nakamura, E., van der Klauw, S.N.G.C., 2004. Ultrahigh-pressure metabasaltic garnets as probes into deep subduction zone chemical cycling. Geochem. Geophys. Geosyst. 5.
Kogiso, T., Tatsumi, Y., Nakano, S., 1997. Trace element transport during dehydration processes in the subducted oceanic crust. 1. Experiments and implications for the origin of ocean island basalts. Earth Planet. Sci. Lett. 148 (1–2), 193–205.
Konrad-Schmolke, M., Zack, T., O'Brien, P.J., Jacob, D.E., 2008. Combined thermodynamic and rare earth element modelling of garnet growth during subduction: examples from ultrahigh-pressure eclogite of the Western Gneiss Region, Norway. Earth Planet. Sci. Lett. 272 (1–2), 488–498.
Lavis, S., 2005. Recycling in Subduction Zones: Evidence from Eclogites and Blueschist of NW China. Cardiff University (1–245 pp.).
Leake, B.E., Woolley, A.R., Arps, C.E.S., Birch, W.D., Gilbert, M.C., Grice, J.D., Hawthorne, F.C., Kato, A., Kisch, H.J., Krivovichev, V.G., Linthout, K., Laird, J., Mandarino, J.A., Maresch, W.V., Nickel, E.H., Rock, N.M.S., Schumacher, J.C., Smith, D.C., Stephenson, N.C.N., Ungaretti, L., Whittaker, E.J.W., Youshi, G., 1997. Nomenclature of amphiboles: Report of the subcommittee on amphiboles of the International Mineralogical Association, Commission on new minerals and mineral names. Am. Mineral. 82, 1019–1037.
Lee, C.T.A., Brandon, A.D., Norman, M., 2003. Vanadium in peridotites as a proxy for paleo-fO(2) during partial melting: prospects, limitations, and implications. Geochim. Cosmochim. Acta 67 (16), 3045–3064.
Lee, C.T.A., Leeman, W.P., Canil, D., Li, Z.X.A., 2005. Similar V/Sc systematics in MORB and arc basalts: implications for the oxygen fugacities of their mantle source regions. J. Petrol. 46 (11), 2313–2336.
Liou, J.G., Tsujimori, T., Zhang, R.Y., Katayama, I., Maruyama, S., 2004. Global UHP metamorphism and continental subduction/collision: the Himalayan model. Int. Geol. Rev. 46 (1), 1–27.
Liu, Y.S., Hu, Z.C., Gao, S., Günther, D., Xu, J., Gao, C.G., Chen, H.H., 2008. *In situ* analysis of major and trace elements of anhydrous minerals by LA-ICP-MS without applying an internal standard. Chem. Geol. 257, 34–43.
Lü, Z., Zhang, L., 2012. Coesite in the eclogite and schist of the Atantayi Valley, southwestern Tianshan, China. Chin. Sci. Bull. 57, 1467–1472.
Lü, Z., Zhang, L.F., Du, J.X., Bucher, K., 2008. Coesite inclusions in garnet from eclogitic rocks in western Tianshan, northwest China: convincing proof of UHP metamorphism. Am. Mineral. 93, 1845–1850.
Lü, Z., Zhang, L.F., Du, J.X., Bucher, K., 2009. Petrology of coesite-bearing eclogite from Habutengsu Valley, western Tianshan, NW China and its tectonometamorphic implication. J. Metamorph. Geol. 27, 773–787.
Lü, Z., Zhang, L., Du, J., Yang, X., Tian, Z., Xia, B., 2012. Petrology of HP metamorphic veins in coesite-bearing eclogite from western Tianshan, China: fluid processes and elemental mobility during exhumation in a cold subduction zone. Lithos 136–139, 168–186.
Lucassen, F., Dulski, P., Abart, R., Franz, G., Rhede, D., Romer, R.L., 2010. Redistribution of HFSE elements during rutile replacement by titanite. Contrib. Mineral. Petrol. 160 (2), 279–295.
Lucassen, F., Franz, G., Dulski, P., Romer, R.L., Rhede, D., 2011. Element and Sr isotope signatures of titanite as indicator of variable fluid composition in hydrated eclogite. Lithos 121 (1–4), 12–24.
Martin, L.A.J., Wood, B.J., Turner, S., Rushmer, T., 2011. Experimental measurements of trace element partitioning between lawsonite, zoisite and fluid and their implication for the composition of arc magmas. J. Petrol. 52 (6), 1049–1075.
Maruyama, S., Cho, M., Liou, J.G., 1986. Experimental investigations of blueschist–greenschist transition equilibria: pressure dependence of Al_2O_3 contents in sodic amphiboles—a new geobarometer. Geol. Soc. Amer. Mem. 164, 17–30.
McCulloch, M.T., Gamble, J.A., 1991. Geochemical and geodynamical constraints on subduction. Earth Planet. Sci. Lett. 102 (3–4), 358–374.
Melzer, S., Wunder, B., 2000. Island-arc basalt alkali ratios: constraints from phengite-fluid partitioning experiments. Geology 28 (7), 583–586.
Mibe, K., Kawamoto, T., Matsukage, K.N., Fei, Y., Ono, S., 2011. Slab melting *versus* slab dehydration in subduction-zone magmatism. Proc. Natl. Acad. Sci. 108 (20), 8177–8182.
Nagasaki, A., Enami, M., 1998. Sr-bearing zoisite and epidote in ultra-high pressure (UHP) metamorphic rocks from the Su-Lu province, eastern China: an important Sr reservoir under UHP conditions. Am. Mineral. 83, 240–247.
Niu, Y.L., 2004. Bulk-rock major and trace element compositions of abyssal peridotites: implications for mantle melting, melt extraction and post-melting processes beneath mid-ocean ridges. J. Petrol. 45, 2423–2458.
Niu, Y.L., Lesher, C.M., 1991. Hydrothermal alteration of mafic metavolcanic rocks and genesis of Fe–Zn–Cu sulfide deposits, Stone Hill District, Alabama. Econ. Geol. Bull. Soc. Econ. Geol. 86 (5), 983–1001.
Niu, Y.L., O'Hara, M.J., 2003. Origin of ocean island basalts: a new perspective from petrology, geochemistry, and mineral physics considerations. J. Geophys. Res. 108 (B4), ECV5.1–ECV5.19.
Pawley, A.R., Holloway, J.R., 1993. Water sources for subduction zone volcanism: new experimental constraints. Science 260, 664–667.
Peacock, S.M., 1990. Fluid processes in subduction zone. Science 248, 329–337.
Plank, T., Langmuir, C.H., 1998. The chemical composition of subducting sediment and its consequences for the crust and mantle. Chem. Geol. 145, 325–394.
Poli, S., Schmidt, M.W., 1995. H_2O transport and release in subduction zones: experimental constraints on basaltic and andesitic systems. J. Geophys. Res. 100 (22), 22,299–22,314 (314).
Poli, S., Schmidt, M.W., 1997. The high-pressure stability of hydrous phases in orogenic belts: an experimental approach on eclogite-forming processes. Tectonophysics 273, 169–184.
Poli, S., Schmidt, M.W., 2002. Petrology of subducted slabs. Annu. Rev. Earth Planet. Sci. 30, 207–235.
Rubatto, D., Hermann, J., 2003. Zircon formation during fluid circulation in eclogites (Monviso, Western Alps): implications for Zr and Hf budget in subduction zones. Geochim. Cosmochim. Acta 67 (12), 2173–2187.
Schmidt, M.W., 1995. Lawsonite: upper pressure stability and formation of higher density hydrous phases. Am. Mineral. 80, 1286–1292.
Schmidt, M.W., Poli, S., 1998. Experimentally based water budgets for dehydrating slabs and consequences for arc magma generation. Earth Planet. Sci. Lett. 163 (1–4), 361–379.
Schmidt, M.W., Vielzeuf, D., Auzanneau, E., 2004. Melting and dissolution of subducting crust at high pressures: the key role of white mica. Earth Planet. Sci. Lett. 228, 65–84.
Schmidt, A., Weyer, S., John, T., Brey, G.P., 2009. HFSE systematics of rutile-bearing eclogites: new insights into subduction zone processes and implications for the earth's HFSE budget. Geochim. Cosmochim. Acta 73 (2), 455–468.
Song, S.G., Su, L., Niu, Y.L., Lai, Y., Zhang, L.F., 2009. CH_4 inclusions in orogenic harzburgite: evidence for reduced slab fluids and implication for redox melting in mantle wedge. Geochim. Cosmochim. Acta 73, 1737–1754.
Sorensen, S.S., Grossman, J.N., Perfit, M.R., 1997. Phengite-hosted LILE enrichment in eclogite and related rocks: implications for fluid-mediated mass transfer in subduction zones and arc magma genesis. J. Petrol. 38, 3–34.
Spandler, C., Hermann, J., Arculus, R., Mavrogenes, J., 2003. Redistribution of trace elements during prograde metamorphism from lawsonite blueschist to eclogite facies; implications for deep subduction-zone processes. Contrib. Mineral. Petrol. 146, 205–222.
Stalder, R., Foley, S.F., Brey, G.P., Horn, I., 1998. Mineral aqueous fluid partitioning of trace elements at 900–1200 degrees C and 3.0–5.7 GPa: new experimental data for garnet, clinopyroxene, and rutile, and implications for mantle metasomatism. Geochim. Cosmochim. Acta 62 (10), 1781–1801.
Staudigel, H., Davies, G.R., Hart, S.R., Marchant, K.M., Smith, B.M., 1995. Large scale isotopic Sr, Nd and O isotopic anatomy of altered oceanic crust: DSDP/ODP sites 417/418. Earth Planet. Sci. Lett. 130, 169–185.
Sun, S.-s, McDonough, W.F., 1989. Chemical and isotopic systematics of oceanic basalts: implications for mantle composition and processes. Geol. Soc. Lond. Spec. Publ. 42 (1), 313–345.
Tatsumi, Y., 1986. Formation of the volcanic front in subduction zones. Geophys. Res. Lett. 13, 717–720.
Tatsumi, Y., Kogiso, T., 2003. The subduction factory: its role in the evolution of the Earth's crust and mantle. In: Larter, R.D., Leat, P.T. (Eds.), Intra-Oceanic Subduction Systems: Tectonic and Magmatic Processes. Geological Society, London, Special Publication, London, pp. 55–80.
Usui, T., Kobayashi, K., Nakamura, E., Helmstaedt, H., 2007. Trace element fractionation in deep subduction zones inferred from a lawsonite–eclogite xenolith from the Colorado Plateau. Chem. Geol. 239, 336–351.
van der Straaten, F., Schenk, V., John, T., Gao, J., 2008. Blueschist-facies rehydration of eclogites (Tian Shan, NW-China): implications for fluid–rock interaction in the subduction channel. Chem. Geol. 255, 195–219.
Volkova, N.I., Budanov, V.I., 1999. Geochemical discrimination of metabasalt rocks of the Fan-Karategin transitional blueschist/greenschist belt, South Tianshan, Tajikistan: seamount volcanism and accretionary tectonics. Lithos 47, 201–216.
Weaver, B.L., 1991. The origin of ocean island end-member compositions: trace element and isotopic constraints. Earth Planet. Sci. Lett. 104, 381–397.
Whitney, D.L., Evans, B.W., 2010. Abbreviations for names of rock-forming minerals. Am. Mineral. 95 (1), 185–187.
Wood, B.J., Bryndzia, L.T., Johnson, K.E., 1990. Mantle oxidation state and its relationship to tectonic environment and fluid speciation. Science 248, 337–345.
Xiao, Y., Lavis, S., Niu, Y., Pearce, J.A., Li, H., Wang, H., Davidson, J., 2012. Trace-element transport during subduction-zone ultrahigh-pressure metamorphism: evidence from western Tianshan, China. Geol. Soc. Am. Bull. 124, 1113–1129.

Xiao, Y., Niu, Y., Song, S., Davidson, J., Liu, X., 2013. Elemental responses to subduction-zone metamorphism: constraints from the North Qilian Mountain, NW China. Lithos 160–161, 55–67.
Zack, T., John, T., 2007. An evaluation of reactive fluid flow and trace element mobility in subducting slabs. Chem. Geol. 239, 199–216.
Zack, T., Rivers, T., Foley, S.F., 2001. Cs–Rb–Ba systematics in phengite and amphibole: an assessment of fluid mobility at 2.0 GPa in eclogites from Trescolmen, Central Alps. Contrib. Mineral. Petrol. 140, 651–669.
Zhang, L.F., Gao, J., Ekebair, S., Wang, Z.X., 2001. Low temperature eclogite facies metamorphism in Western Tianshan, Xinjiang. Sci. China 44 (1), 85–96.
Zhang, L.F., Ellis, D.J., Jiang, W.B., 2002. Ultrahigh-pressure metamorphism in western Tianshan, China: part I. Evidence from inclusions of coesite pseudomorphs in garnet and from quartz exsolution lamellae in omphacite in eclogites. Am. Mineral. 87, 853–860.
Zhang, L.F., Ellis, D.J., Arculus, R.J., Jiang, W., Wei, C., 2003. 'Forbidden zone' subduction of sediments to 150 km depth—the reaction of dolomite to magesite + aragonite in the UHPM metapelites from western Tianshan, China. J. Metamorph. Geol. 21, 523–529.
Zindler, A., Hart, S., 1986. Chemical geodynamics. Ann. Rev. Earth Planet. Sci. 14, 493–571.